iScience

CellPress
OPEN ACCESS

Article

LncNSPL facilitates influenza A viral immune escape by restricting TRIM25-mediated K63-linked RIG-I ubiquitination

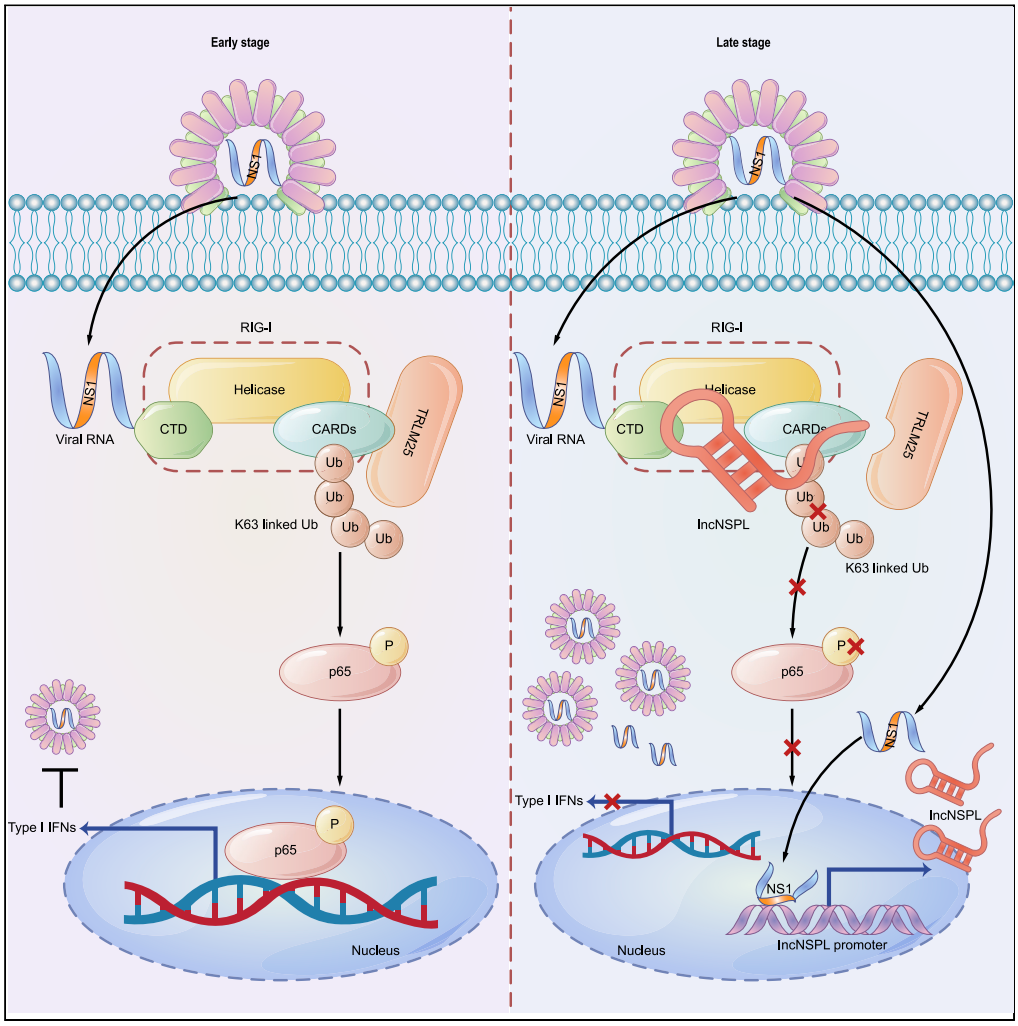

Jingjing Jiang, Yuyu Li, Zeyu Sun, ..., Yuchong Wang, Xiaoling Su, Hongyan Diao

diaohy@zju.edu.cn

Highlights

NS1 protein of Influenza A virus (IAV) promotes lncNSPL expression

Deficiency of lncNSPL specifically enhances retinoic acid-inducible gene I (RIG-I) initiated IFN production

lncNSPL competes with tripartite interaction motif 25 (TRIM25) for binding RIG-I and inhibits its K63 ubiquitination

lncNSPL inhibits innate antiviral immune responses and enhances viral replication

Jiang et al., iScience 25, 104607
July 15, 2022
https://doi.org/10.1016/j.isci.2022.104607

iScience

CellPress
OPEN ACCESS

Article

LncNSPL facilitates influenza A viral immune escape by restricting TRIM25-mediated K63-linked RIG-I ubiquitination

Jingjing Jiang,[1] Yuyu Li,[1] Zeyu Sun,[1] Lan Gong,[2] Xuehui Li,[1] Fan Shi,[1] Jian Yao,[1] Yuting Meng,[1] Xiaohua Meng,[1] Qiong Zhang,[1] Yuchong Wang,[1] Xiaoling Su,[1] and Hongyan Diao[1,3,*]

SUMMARY

Long noncoding RNAs (lncRNAs) participate in host antiviral responses; however, how viruses exploit host lncRNAs for immune evasion remains largely unexplored. Functional screening of differentially expressed lncRNA profile in patients infected with influenza A virus (IAV) revealed that lncNSPL (Gene Symbol: LOC105370355) was highly expressed in monocytes. Deregulated lncNSPL expression in infected monocytes significantly increased type I interferon (IFN-I) production and inhibited IAV replication. Moreover, lncNSPL overexpression in mice increased the susceptibility to IAV infection and impaired IFN-I production. LncNSPL directly bound to retinoic acid-inducible gene I (RIG-I) and blocked the interaction between RIG-I and E3 ligase tripartite interaction motif 25 (TRIM25), reducing TRIM25-mediated lysine 63 (K63)-linked RIG-I ubiquitination and limiting the downstream production of antiviral mediators during the late stage of IAV infection. Our findings provide mechanistic insights into the means by which lncNSPL promotes IAV replication and immune escape via restricting the TRIM25-mediated RIG-I K63-linked ubiquitination. Thus, lncNSPL may represent a promising pharmaceutical target for anti-IAV therapy.

INTRODUCTION

Influenza virus infections, including influenza A virus (IAV) infection, cause as many as 3-5 million cases of severe illness and 250,000-500,000 deaths every year worldwide (Gopal et al., 2020). Therefore, this RNA virus poses a significant threat to global public health. It has been established that IAV surface proteins mutate rapidly and can combine into dozens of variants; thus, an IAV pandemic represents a substantial threat (Richard et al., 2016). Although remarkable progress has been made to explore the human defense system by which host innate antiviral immunity is generated (Chen et al., 2021b), the detailed molecular mechanisms underlying IAV-host interactions, especially the viral counterpart, remain elusive.

Influenza A virus damages the respiratory tract and lungs of humans and animals are extensively studied. During IAV infection, the innate immune system provides the first line of host defense against invading pathogens (Tan et al., 2018). Moreover, monocyte-macrophages represent frontline immune cells involved in the coordination of innate immunity and are major producers of inflammatory mediators during an antiviral response (Nikitina et al., 2018; Wang et al., 2022). The host primarily detects IAV invasion through retinoic acid-inducible gene I (RIG-I), a cytosolic pattern recognition receptor (PRR) that recognizes cytoplasmic RNA viruses and initiates an antiviral immune response. RIG-I protein contains two caspase recruitment domains (CARDs) in the N-terminus, an RNA helicase domain with an ATP-binding motif, and a C-terminal domain (CTD) (Jiang et al., 2011). Ubiquitination is a key post-translational modification (PTM) during the activation of a RIG-I-mediated innate immune response (Liu et al., 2016). For instance, the E3 ubiquitin ligase tripartite interaction motif 25 (TRIM25) interacts with the RIG-I CARD domain and mediates lysine 63 (K63)-linked ubiquitination of RIG-I, which is crucial for the RIG-I downstream signaling and the antiviral innate immune response (Gack et al., 2007). K63-ubiquitinated RIG-I interacts with the signaling adaptor mitochondrial antiviral signaling (MAVS) protein to activate the transcription factors interferon regulatory factor 3 (IRF3) and nuclear factor κB (NF-κB), which then initiates the subsequent production of type I interferon (IFN-I) (Hou et al., 2011).

[1]State Key Laboratory for Diagnosis and Treatment of Infectious Diseases, National Clinical Research Center for Infectious Diseases, Collaborative Innovation Center for Diagnosis and Treatment of Infectious Diseases, The First Affiliated Hospital, College of Medicine, Zhejiang University, Hangzhou, China

[2]Microbiome Research Centre, St George and Sutherland Clinical School, University of New South Wales, Sydney, NSW 2052, Australia

[3]Lead contact

*Correspondence: diaohy@zju.edu.cn

https://doi.org/10.1016/j.isci.2022.104607

Several pathogens, including IAV, have evolved a variety of molecular strategies to evade or counteract the host immune response (Haller et al., 2006; Zhang et al., 2021). Nonstructural protein 1 (NS1) has been found to be an effective IFN antagonist against anti-IAV immunity (Krug, 2015; Zhang et al., 2022). A recent study reported that NS1 interacts with TRIM25 and efficiently suppresses TRIM25-induced RIG-I ubiquitination and activation (Gack et al., 2009). In addition, NS1 interacts with the RNA helicase domain of RIG-I and inhibits the downstream activation of IRF3 (Mibayashi et al., 2007); however, the detailed molecular mechanism by which the NS1 protein antagonizes the function of RIG-I is unclear.

Long noncoding RNAs (lncRNAs) are emerging as important regulators of both innate and adaptive immunity (Yao et al., 2021). Increased research attention has been paid to the functions of lncRNAs in the host immune response against viral infections. For instance, lnc-Lsm3b has been shown to compete with viral RNAs for binding to RIG-I and acts as a potent molecular decoy to restrict the host's viral RNA-induced innate immune response (Jiang et al., 2018). The mechanism by which lncRNAs act as competitors to weaken RIG-I-TRIM25 interaction has not been reported yet. Another lncRNA lnc-AAM functions as a transcription enhancer to activate macrophages and promote adaptive immunity (Chen et al., 2021c). Despite the occasional reports of lncRNA-mediated manipulation of host immunity, how the virus utilizes lncRNAs to evade elimination by the monocyte-macrophages system remains poorly understood.

In the present study, we profiled lncRNAs in IAV-infected patients and identified a new lncRNA with upregulated expression in monocytes on IAV infection. Further investigation revealed that the IAV NS1 protein could promote the expression of this lncRNA, and it was hence termed NS1-promoted lncRNA (lncNSPL). Altering the level of lncNSPL significantly affected the production of antiviral IFN-I protein and facilitated viral replication both *in vitro* and *in vivo*. Cytoplasmic lncNSPL can bind to RIG-I and block the interaction between RIG-I and TRIM25, which prevents TRIM25-mediated K63-linked ubiquitination of RIG-I and consequently suppresses the activation of the downstream antiviral innate response. In general, as an inhibitor of the host's antiviral immunity in monocytes, lncNSPL promotes viral replication and immune escape. These results indicate that lncNSPL plays a key role in the process of IAV infection.

RESULTS

Cytosolic RNA sensor retinoic acid-inducible gene I initiates an antiviral immune response in influenza A virus-infected patients

The transcriptomic profiles of both messenger RNAs (mRNAs) and lncRNAs were obtained from IAV-infected patients and healthy controls (HCs) (see Table S1). A total of 585 upregulated and 2,732 downregulated mRNAs (fold-change > 1.5, $p < 0.01$) were detected and clustered (Figure 1A). The Kyoto Encyclopedia of Genes and Genomes (KEGG) pathway analysis demonstrated that the RIG-I-like receptor signaling pathway was significantly over-represented in the upregulated genes (Figure 1B, right). The alluvial diagram showed that the up-regulation of CLCL10, RIG-I, ISG15, and NFKBIA mRNAs were enriched in the RIG-I-like receptor signaling pathway (Figure 1C, left). As an important host sensor for RNA viruses, RIG-I plays a key role in viral recognition and immune responses against viral infection including IAV invasion (Rehwinkel and Gack, 2020). Furthermore, the gene expression profiles related to RIG-I were used to analyze the co-expression models from the Gene Expression Omnibus (GEO) database using the WGCNA R package (Figure 1C). These analyses highlighted the versatility of RIG-I in the host defense response to eliminate invading IAVs. Importantly, the level of RIG-I mRNA was substantially elevated in the IAV-infected patients compared with the HCs (Figure 1D), which was further validated in another cohort retrieved from the GEO database (Figure 1E).

Other PRR RNA sensors, such as toll-like receptor 7 (TLR7) and TLR8, can detect IAV infection by recognizing ssRNA ligands (de Marcken et al., 2019). The qRT-PCR results indicated that IAV infection upregulated the expression of TLR7 and TLR8 in IAV-infected patients, but with a much smaller increase compared to the up-regulation of PRR RNA sensor RIG-I (Figures S1A, S1B, and 1D). These results were validated *in vivo* in three independent cohorts retrieved from the GEO database (Figures S1C-S1E) and *in vitro* in cultured human monocytes THP-1 cells infected with IAV subtype H1N1 (Figure 1F). We also evaluated the potential accuracy of RIG-I as a biomarker for detecting IAV infection and stimulating antiviral response using generated ROC curves. The area under the curve (AUC) indicated the successful prognostic classification based on the RIG-I risk score (AUC = 0.909), higher than the prediction accuracy of TLR7 and TLR8 (AUC = 0.671, 0.646) (Figure 1G). This prediction model was validated in two independent cohorts retrieved from the GEO database (Figures S1F and S1G). Taken together, the above data suggest that the PRR RNA sensor RIG-I plays a critical role in monitoring invading IAV and initiating antiviral innate immune responses to eliminate virus.

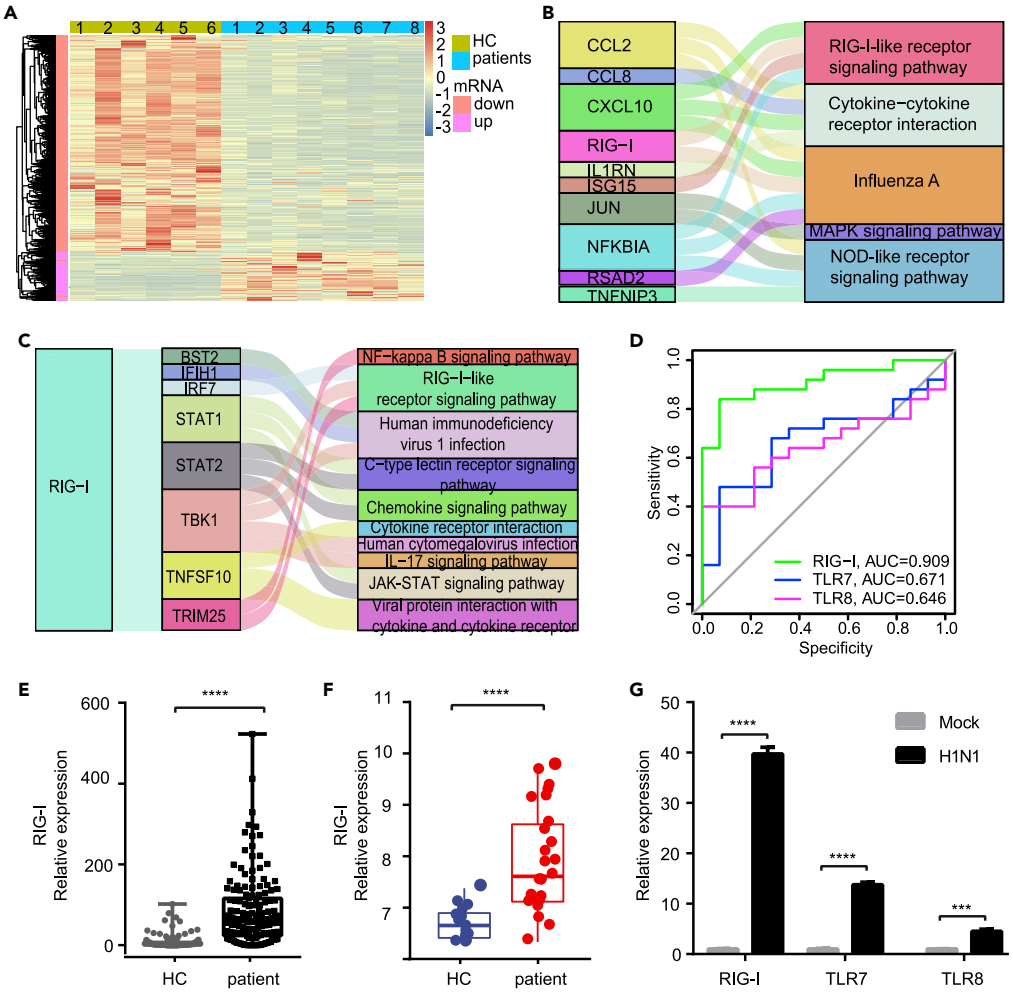

Figure 1. mRNA profiling of IAV-infected patients revealed that RIG-I was significantly upregulated

(A) Cluster heatmap showing significantly differential levels of mRNAs in IAV-infected patients (n = 8) and healthy controls (HCs) (n = 6). The coloring provides an overview of numeric differences (fold-change > 1.5, $p < 0.01$).

(B) An alluvial diagram represents the 10 genes involved in the top five IAV-related pathways.

(C) The gene expression profiles related to RIG-I were used to analyze the co-expression models from the GEO database.

(D) RIG-I expression was measured in IAV-infected patients and healthy controls (HCs) by qRT-PCR analysis (HCs: n = 147; patients: n = 162; ****$p < 0.0001$).

(E) The levels of RIG-I expression retrieved from the GEO database (cohort GSE100150) were analyzed (HCs: n = 14; patients: n = 25; ****$p < 0.0001$).

(F) qRT-PCR analysis of RIG-I, TLR7, and TLR8 expression in THP-1 cells infected with IAV-H1N1 for 12 h (***$p < 0.001$, ****$p < 0.0001$).

(G) ROC curve analysis of predicting IAV infection based on the RIG-I, TLR7, and TLR8 expression in the cohort GSE100150 retrieved from the GEO database, risk score shown as AUC.

Identification of novel long noncoding RNA lncNSPL in the anti-influenza A virus innate response

LncRNAs modulate various biological processes including innate and adaptive immunity; however, their roles in host anti-IAV innate responses are largely unknown. In the above transcriptomic profiles of lncRNAs, a total of 1,650 differentially expressed lncRNA transcripts (fold-change > 2.0; $p < 0.05$) were identified between the IAV-infected patients and the HCs, including 344 up-regulated and 1,306 down-regulated lncRNA transcripts (Figure 2A). To elucidate the potential association of these lncRNA transcripts with RIG-I expression, we performed a correlation analysis between lncRNA transcripts and RIG-I using a Pearson correlation coefficient assay (Figure 2B). Three lncRNAs were identified as most

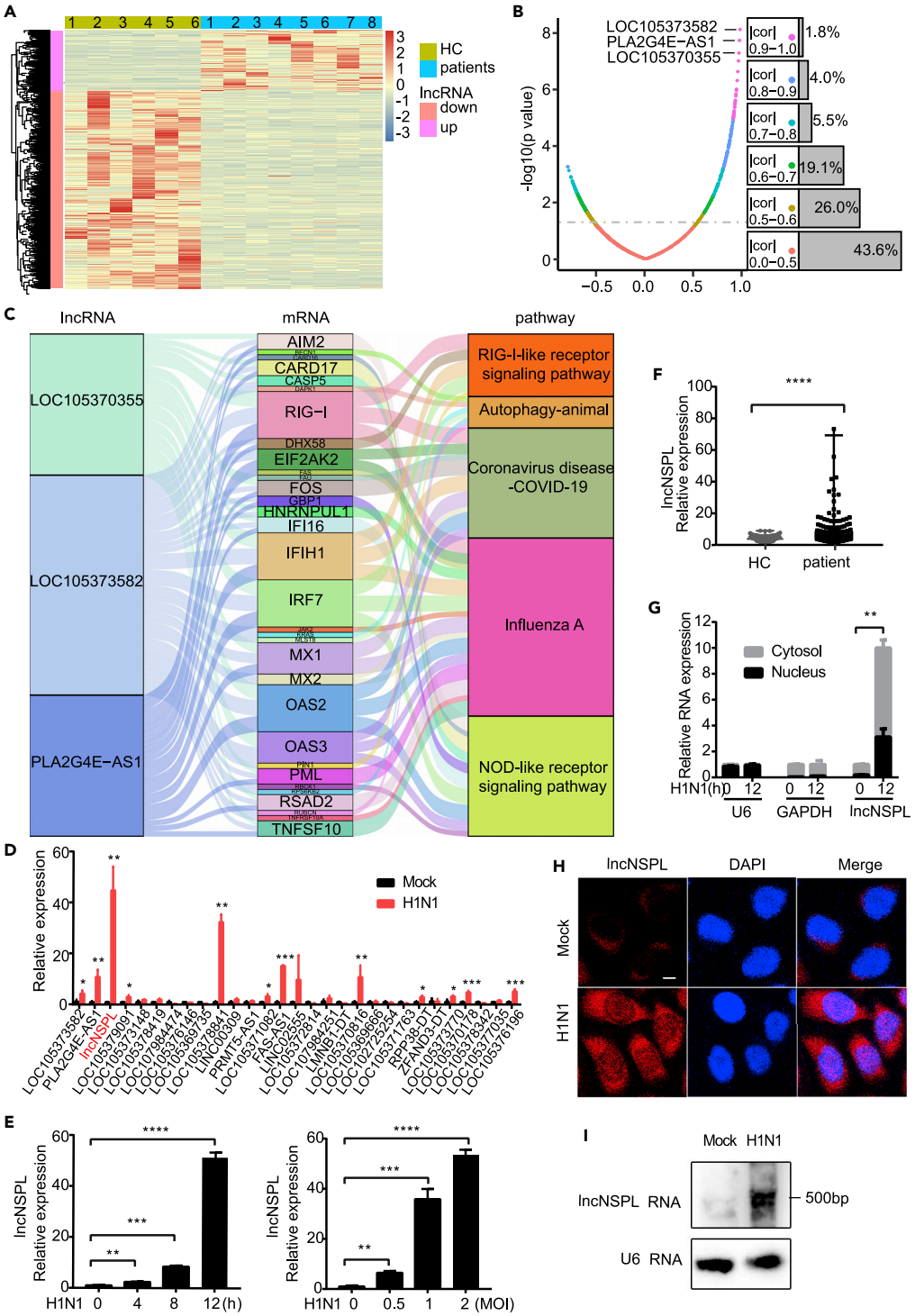

Figure 2. Identification and characterization of lncNSPL in the anti-IAV innate response

(A) Sequencing analysis revealed 344 up-regulated and 1,306 down-regulated lncRNA transcripts in transcriptomic profiles of IAV-infected patients (n = 8) and HCs (n = 6). The coloring provides an overview of numeric differences (fold-change > 1.5, $p < 0.01$).

(B) Pearson correlation coefficient of all differentially expressed lncRNAs with RIG-I showing three most related lncRNAs: LOC105373582, LOC105370355, and PLA2G4E−AS1 (cor >0.96; $p < 0.01$).

Figure 2. *Continued*

(C) Alluvial diagram showing the association of the five most significant pathways with these three RIG-I-related lncRNAs and their predicted target genes.

(D) qRT-PCR verification of 29 upregulated lncRNAs closely related to RIG expression (cor >0.9; $p < 0.01$) in THP-1 cells infected with or without IAV-H1N1 (*$p < 0.05$, **$p < 0.01$, ***$p < 0.001$).

(E) qRT-PCR analysis of lncNSPL expression in THP-1 cells infected with IAV-H1N1 strain PR8 for the indicated dose (0-2 MOI) or time period (0-12 h) (**$p < 0.01$, ***$p < 0.001$, ****$p < 0.0001$).

(F) Real-time qRT-PCR validation of lncNSPL expression in samples of IAV-infected patients and healthy controls (HCs) (HCs: n = 147; patients: n = 162,****$p < 0.0001$).

(G) qRT-PCR analysis of the indicated RNA levels of U6, GAPDH, and lncNSPL in the cytosolic or nuclear subcellular fraction in THP-1 cells with or without IAV-H1N1 infection (**$p < 0.01$).

(H) Confocal fluorescence microscopy images of lncNSPL stained with the FISH probe (red) in THP-1 cells on H1N1 infection for the indicated time period. Nuclei were stained with DAPI (blue). Scale bar: 10 μm.

(I) Northern blotting of lncNSPL in THP1 cells treated with mock or PR8 (MOI = 1) at 12 h post-infection.

related to RIG-I: LOC105373582, LOC105370355, and PLA2G4E−AS1 (cor >0.96; $p < 0.01$). Next, we predicted the target mRNAs of these three lncRNAs using the RNA Interactome Database (RAID v 3.0). Five upregulated KEGG pathways were correlated with these target mRNAs including RIG-I (Figure 2C): RIG-I-like receptor signaling pathway, autophagy, coronavirus disease-COVID-19, influenza A, and NOD-like receptor signaling pathway. Furthermore, a gene set variation analysis (GSVA) indicated that LOC105370355, LOC105373582, and PLA2G4E−AS1 were significantly positively correlated with the RIG-I and RIG-I-like receptor signaling pathway (Figure S2). Importantly, a qRT-PCR assay of 29 lncRNAs confirmed that one novel lncRNA (Gene Symbol: LOC105370355), termed lncNSPL, was most significantly upregulated in IAV-infected THP-1 human monocytes (Figure 2D). We also observed that this *in vitro* upregulation of lncNSPL in response to IAV was both infection time- and dose-dependent (Figure 2E). Interestingly, we found that infection with a high concentration of IAV subtype H1N1 for a relatively long period (at least 8 h) was required to significantly induce lncNSPL expression. The *in vivo* validation of IAV-induced lncNSPL was performed by qRT-PCR showing that lncNSPL was significantly upregulated in IAV-infected patients (Figure 2F). In addition, we confirmed that lncNSPL could be stimulated by other sub-strain of IAV H3N2 in a dose-dependent manner (Figure S3A). To further investigate the role in lncNSPL in the innate immune response, we monitored lncNSPL expression in THP-1 cells treated with other respiratory viruses, including infection with RNA viruses (a seasonal human β-coronavirus HCoV-OC43), the DNA virus herpes simplex virus 1 (HSV-1). However, following these stimuli, we failed to observe any significant upregulation of lncNSPL expression (Figure S3B). These results may further demonstrate an important and selective role of lncNSPL in regulating innate immune responses against IAV viral infection. No protein-coding potential was detected in lncNSPL by further analysis using an NCBI ORF finder (https://www.ncbi.nlm.nih.gov/orffinder/) (Figure S4) and coding potential score calculator (score: 0.038) (http://lilab.research.bcm.edu/cpat/). Subcellular localization followed by qRT-PCR in THP-1 cells with or without H1N1 infection showed that lncNSPL was predominantly localized in the cytoplasm (Figure 2G), which was subsequently confirmed by an RNA fluorescence *in situ* hybridization (RNA-FISH) analysis (Figure 2H). Only one transcript of AVAN was found and it was upregulated on H1N1 infection using northern blot analysis (Figure 2I). These findings collectively suggest that IAV infection stimulates the cytosolic accumulation of a novel lncRNA lncNSPL which might exert regulatory effects through binding to functional cytoplasmic proteins.

LncNSPL is stimulated by influenza A virus NS1 protein and accumulated in activated monocytes

It has previously been reported that the expression of host noncoding RNAs including lncRNAs can be regulated by viral proteins (Chen et al., 2021a). Thus, we further examined which IAV proteins could stimulate lncNSPL expression. The genome of H1N1 consists of 8 negative-sense, single-stranded viral RNA (vRNA) segments, coding for at least eight essential proteins (Palese and Schulman, 1976). We found that seven other proteins (HA, NA, NP, M1, PB2, PB1, and PA) from the PR8 strain had no effect on lncNSPL expression (Figure 3A). Only overexpression of the IAV nonstructural 1 (NS1) protein from the PR8 strain remarkably upregulated lncNSPL expression in a dose-dependent manner, as did the NS1 protein from the California/07/2009 strain of IAV (Figures 3A and S5A). Correspondingly, the lncNSPL promoter (approximately 2,000bp upstream of the ATG start codon of the human loc105370355 gene) could be activated by the IAV NS1 protein (from both PR8 and California/07/2009 strains) in human HEK293T cells (Figures 3B and S5B); and it was, therefore, termed NS1 promoted lncRNA (lncNSPL). An RNA-FISH analysis revealed that the lncNSPL copy number was increased along with an elevated amount of NS1 during the late stage of

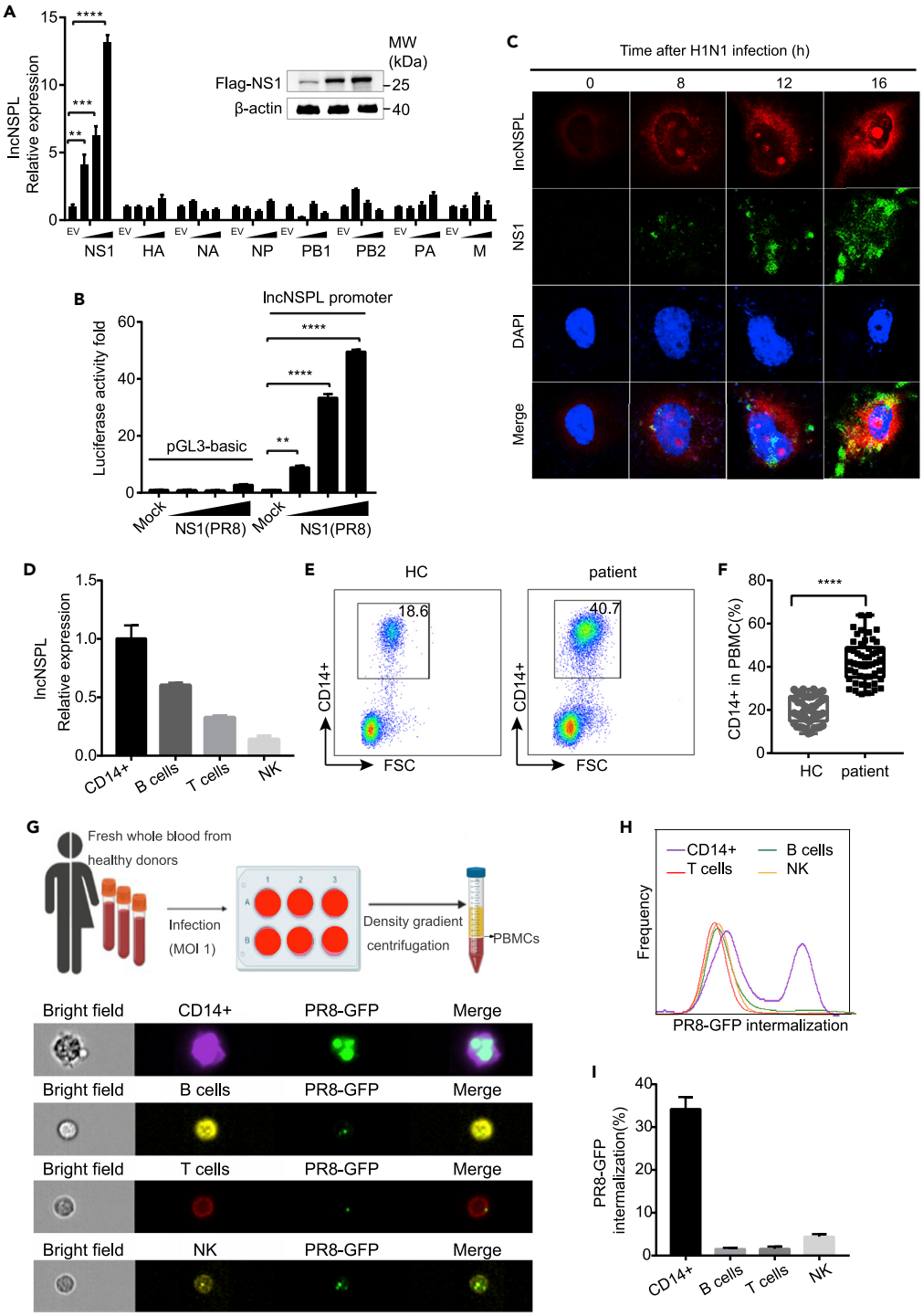

Figure 3. LncNSPL is stimulated by IAV NS1 protein and highly expressed in activated monocytes

(A) LncNSPL expression was measured by qRT-PCR in THP-1 cells transfected with plasmids expressing IAV (PR8 strain) viral protein NS1, HA, NA, NP, PB1, PB2, PA, M (**p < 0.01, ***p < 0.001, ****p < 0.0001). The immunoblot analysis showed that different concentrations of Flag-NS1 plasmids produced a gradually increasing amount of NS1 proteins.

(B) LncNSPL promoter activity in HEK293T cells co-transfected with the plasmids lncNSPL-promoter and/or IAV (PR8 strain) NS1 (at different doses) (**p < 0.01, ***p < 0.001, ****p < 0.0001).

(C) NS1 (green) facilities the expression of cytoplasmic lncNSPL (red) stained with the FISH probe in THP-1 cells with H1N1-PR8 infection at the indicated time points (0-16 h). Nuclei were stained with DAPI (blue). Scale bar: 10 μm.

Figure 3. *Continued*

(D) qRT-PCR analysis of lncNSPL expression in the indicated human immune cells, $CD14^+$ monocytes, $CD3^+$ T cells, B cells, and NK cells, that were isolated from PBMCs. Data are representative of three independent experiments (n = 3 technical replicates).

(E and F) Flow cytometry profiling of a $CD14^+$ monocyte subset of PBMCs from IAV-infected patients (n = 50) and HCs (n = 50). Representative FACS plots are shown in (E) and the relative percentage of this subset in PBMCs is depicted in the bar chart (F) (****$p < 0.0001$).

(G) PBMCs were isolated from the whole blood derived from healthy donors (n = 6), followed by IAV-H1N1 (PR8 NS1-GFP) infection at an MOI of one for 24 h and imaging flow cytometry was used to detect H1N1 target cells. Schematic representation of the experimental set-up.

(H) Imaging of the flow cytometry profiling of $CD14^+$ monocytes, $CD3^+$ T cells, B cells, and NK cells with H1N1 (PR8 NS1-GFP) infection.

(I) H1N1 infection efficiency in various immune cells was calculated as PR8-GFP internalization (%) from the data of imaging flow cytometry.

IAV-H1N1 infection (8-16h post-infection) (Figure 3C). LncNSPL was widely expressed in multiple types of immune cells (Figure 3D), in which lncNSPL was expressed at highest level in $CD14^+$ monocytes while at relatively low levels in other immune cells such as $CD3^+$ T cells, B cells, and natural killer (NK) cells. Interestingly, flow cytometry results showed that the proportion of $CD14^+$ monocytes in the peripheral blood mononuclear cells (PBMCs) of IAV-infected patients was significantly increased compared with HCs (more than 2-fold increase from 18.6% to 40.7%) (n = 50) (Figures 3E and 3F). As reported previously, circulating monocytes could infiltrate inflamed tissues where they differentiate into monocyte-derived macrophages (MDM). Cluster of differentiation 14 (CD14) was described as a monocyte/macrophage differentiation antigen on the surface of myeloid lineages, such as monocytes, macrophages, and dendritic cells (DCs) (Wynn et al., 2013). Macrophages are key players in tissue homeostasis and inflammation. Macrophages have roles in almost every aspect of an organism's biology ranging from development, homeostasis, to repair through to immune responses to pathogens (Russell et al., 2019). Activated macrophages are key producers of inflammatory cytokines in the blood and play an important role in the innate defense against viral infection (Murray and Wynn, 2011). Moreover, IAV-infected patients displayed a decreased portion of $CD3^+CD8^+$ T cells in PBMCs compared to HCs (Figures S6A and S6B).

Previous studies have shown that IAV infects epithelial cells of lung. To better understand the dynamics of IAV infection progression, and to identify the specific cell types susceptible to IAV infection. We gated isolated PBMCs from infected blood by imaging flow cytometry. Whole blood infections obtained from healthy donors were performed using a recombinant IAV-H1N1 strain PR8 carrying a GFP reporter gene tagged to the NS1 segment (PR8 NS1-GFP) at a multiplicity of infection (MOI) of 1 (Figure 3G, up). At 12 h post-infection, PBMCs were isolated from whole-blood specimens and the susceptibility of IAV infection was determined using imaging flow cytometry. The isolated PBMCs were gated into four major subsets of peripheral blood immune cells (monocytes, B cells, T cells, and NK cells). A significantly higher intensity of GFP fluorescence was detected in the $CD14^+$ monocytes (more than 30%) compared to those in B cells, T cells, and NK cells (Figures 3G-3I). Imaging flow cytometry analyses indicated that among these immune subsets, $CD14^+$ monocytes are more susceptible to IAV infection. All these results indicate that lncNSPL is stimulated by IAV NS1 protein and highly expressed in activated monocytes.

LncNSPL suppresses antiviral type I interferons and promotes influenza A virus replication

To further determine the function of lncNSPL in an IAV infection, we transiently depleted lncNSPL in IAV-infected THP-1 cells using siRNA (si-lncNSPL), which was confirmed by qRT-PCR (Figure S7A). A specific knockdown of lncNSPL significantly increased the production of antiviral cytokines, including IFN-β, IL-6, and IL-1β in 12-myristate 13-acetate (PMA)-differentiated THP-1 macrophages at both the RNA (Figure 4A) and protein (Figure 4B) levels following IAV-H1N1 infection. To further confirm the role of lncNSPL, we generated the THP-1 cell line that stably expressed either whole length lncNSPL (LV-lncNSPL cells) (Figure S7B) or specific shRNA targeting lncNSPL (sh-lncNSPL cells). In contrast, the expressions of IFN-β, IL-6, and IL-1ββdecreased correspondingly in the LV-lncNSPL cells on IAV infection compared to the empty vector cells (EV cells) (Figures S8A and S8B). Notably, the reintroduction of lncNSPL into the lncNSPL-deficient cells also markedly decreased the IAV-induced expression of IFN-β, IL-6, and IL-1β (Figure S8C). These data indicate that lncNSPL plays an important role in the host's anti-IAV innate defense by negatively modulating antiviral genes such as IFN-β, IL-6, and IL-1β. Strikingly, lncNSPL-deficient THP-1 cells (silncNSPL) displayed a significantly decreased viral titer following an IAV-H1N1 infection, as indicated in

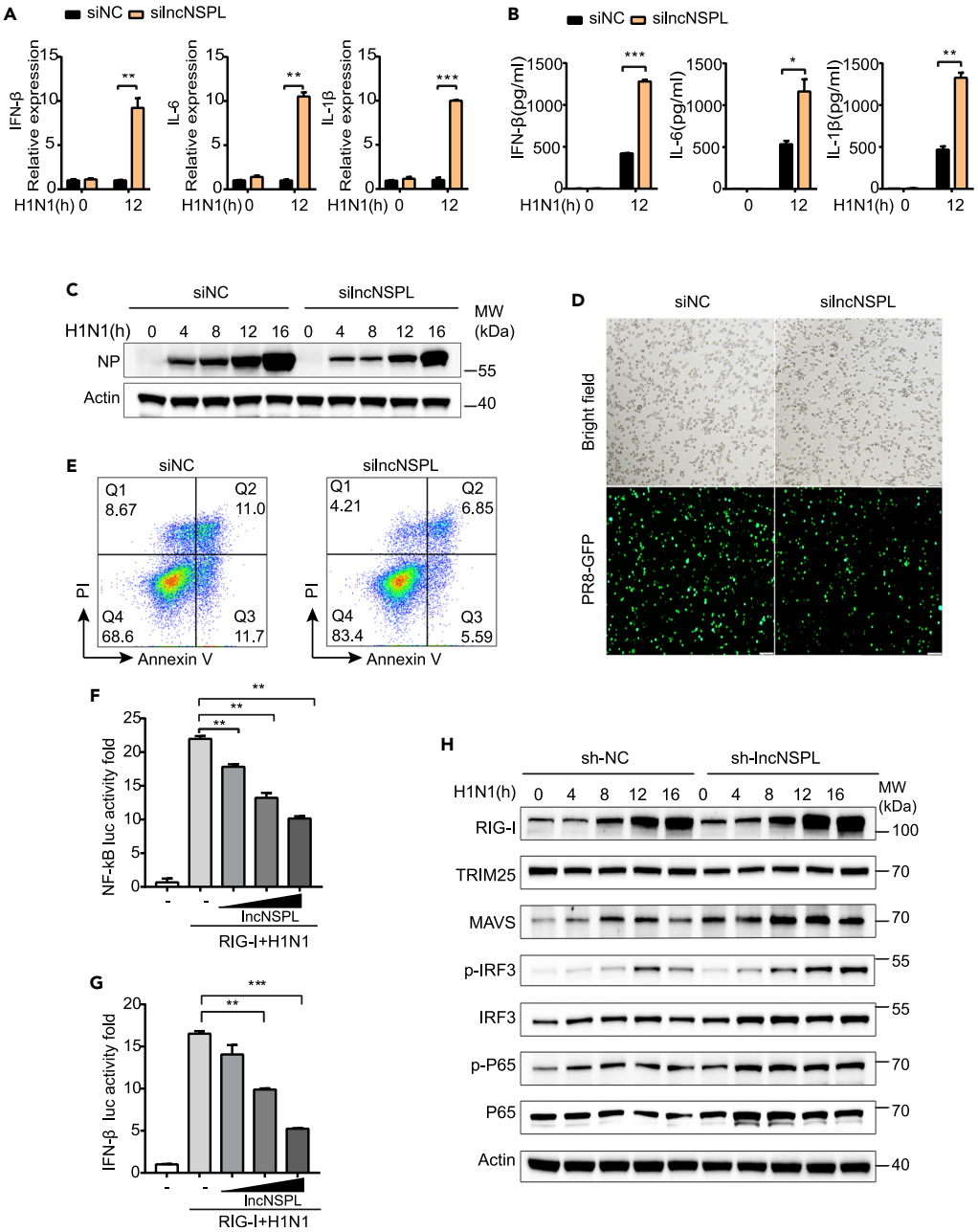

Figure 4. LncNSPL suppresses RIG-I-mediated type I IFN production and promotes IAV replication

(A) Expression of IFN-β, IL-6, and IL-1β at mRNA levels in PMA-differentiated THP-1 macrophages transfected with control siRNA (siNC) or siRNA targeting lncNSPL (silncNSPL) for 48 h, and subsequently infected with H1N1 for indicated time (*p < 0.05, **p < 0.01, ***p < 0.001).

(B) ELISA results showing the protein levels of IFN-β, IL-6, and IL-1β in the supernatants of THP-1 cells transfected with siNC or silncNSPL for 48 h before H1N1 infection for 12 h (*p < 0.05, **p < 0.01, ***p < 0.001).

(C) The level of viral NP expression was analyzed by Western blot in THP-1 cells transfected with siNC or silncNSPL for 48 h and infected with H1N1 for the indicated time periods (0-16h). Actin as an internal control.

(D) Fluorescence microscopy images of viral replication (green, PR8-GFP) in siNC or silncNSPL-transfected THP-1 cells infected with GFP-tagged H1N1 for 12 h. Data are representative of three independent experiments (n = 3 technical replicates).

(E) Apoptosis was measured by PI-Annexin V FACS assay in A549 cells co-cultured with the supernatant of siNC or silncNSPL-transfected THP-1 cells infected with H1N1 for 12h.

Figure 4. *Continued*

(F and G) NF-κB (F) and IFN-β (G) promoter activities were measured in HEK293T cells transfected with lncNSPL of different doses and RIG-I vectors followed by H1N1 infection (**$p < 0.01$, ***$p < 0.001$).

(H) Western blot showing the levels of key proteins in the RIG-I signaling pathway in THP-1 cells stably transfected with control shRNA (sh-NC) or shRNA targeting lncNSPL (sh-lncNSPL) and infected with H1N1 for the indicated time periods (0-16 h).

the level of viral nucleoprotein (NP) (Figure 4C). Consistently, compared to the control cells, a knockdown of lncNSPL restricted the replication of GFP-tagged IAV-PR8 strain (Figure 4D). This decrease in the viral load was likely owing to a heightened host innate immune response, as the production of antiviral cytokines including IFN-β, IL-6, and IL-1β was increased by the knockdown of lncNSPL. A549 human alveolar basal epithelial cells co-cultured with the supernatant of lncNSPL-deficient THP-1 cells infected with IAV exhibited significantly reduced apoptosis (Figure 4E). In contrast, the viral titer was significantly upregulated in the LV-lncNSPL cells on IAV infection (Figures S8D and S8E), and the supernatant of the LV-lncNSPL cells infected with IAV could promote apoptosis in A549 cells (Figure S8F). These results combinedly suggest that monocytes-derived lncNSPL may be involved in the negative regulation of IFN-I-mediated antiviral responses leading to higher IAV replication. We isolated $CD14^+$ monocyte/$CD14^-$cells from PBMCs, which were cell cultured and infected with H1N1 for 12h. Then A549 were co-cultured with the supernatants of $CD14^+$ monocyte/$CD14^-$cells, respectively. The result showed that the apoptosis of A549 cells was significantly enhanced after co-culture with $CD14^+$ monocyte supernatant (Figure S9). This result indicated that the monocytes-derived lncNSPL may play an important role in influenza virus infection.

In addition, in A549 cells, the lncNSPL was also increased in response to H1N1 infection (Figure S10A) and its silencing resulted in increased IFN-β, IL-6, and IL-1β production (Figure S10B) and suppressed viral replication (Figure S10C) on H1N1 viral infection. LncNSPL overexpression showed the opposite effect in A549 cells (Figures S10D and S10E). These results may suggest that the function of lncNSPL in promoting H1N1 replication might be not only observed in human immune cells.

LncNSPL inhibits retinoic acid-inducible gene I-induced nuclear factor κB and interferon-β activation

To gain insight into the mechanism by which lncNSPL suppresses IFN-I production, we investigated the effects of lncNSPL on the upstream events such as RIG-I-induced activation of nuclear factor κB (NF-κB) and IFN-β. It was shown that lncNSPL inhibited the luciferase reporter activation of both RIG-I-induced NF-κB (Figure 4F) and IFN-β (Figure 4G) in HEK293T cells in a dose-dependent manner, suggesting that lncNSPL might target RIG-I for IFN-I production. Furthermore, we found that the levels of phosphorylated RIG-I-related regulators IRF3 and p-P65 were both significantly higher in lncNSPL-deficient THP-1 cells compared to the controls from 8 h to 24 h post-H1N1 infection (Figure 4H). In contrast, lncNSPL overexpression inhibited the H1N1-induced phosphorylation/activation of IRF3, NF-κB-P65 in the IAV-infected LV-lncNSPL cells (Figure S11). Collectively, these data suggest that lncNSPL selectively attenuates RIG-I-induced NF-κB and IFN-β activation, leading to an inhibition of downstream signaling such as IFN-I production. In addition, LV-lncNSPL cells with small interfering (siRNA)-mediated knockdown of RIG-I displayed a significantly increased H1N1 viral replication, both at the viral RNA and protein level (Figure S12).

LncNSPL-overexpressing mice are more vulnerable to influenza A virus infection with low interferon-I production

LncNSPL is not conserved between humans and mice. To further investigate the detailed effect of lncNSPL on IAV infection in the mouse model, we first generated an *in vitro* lncNSPL-overexpression system using murine macrophage cell line RAW264.7. Compared to empty vector (EV)-overexpressing cells, lncNSPL-overexpressing RAW264.7 cells exhibited reduced production of IFN-β, IL-6, and IL-1β following IAV infection, implying that the negative regulation of IFN-I production by lncNSPL was observed in both human and mouse immune cells (Figure 5A). These results suggest that the role of lncNSPL in inhibiting IFN-I production may be conserved between humans and mice. Next, we generated lncNSPL-overexpressing mice (AAV-lncNSPL) via an intravenous (i.v.) injection via the tail vein with a high dose of lncNSPL-containing adeno-associated virus (AAV) (Lai et al., 2021). At 21 days post-injection, the AAV-lncNSPL mice displayed significantly elevated levels of lncNSPL expression in the lung compared with the controls (AAV-Vector) (Figures S13A and S13B). The AAV-lncNSPL mice did not display changes in body weight or activity compared to their AAV-Vector control littermates (data not shown). After being intranasally (i.n.) inoculated

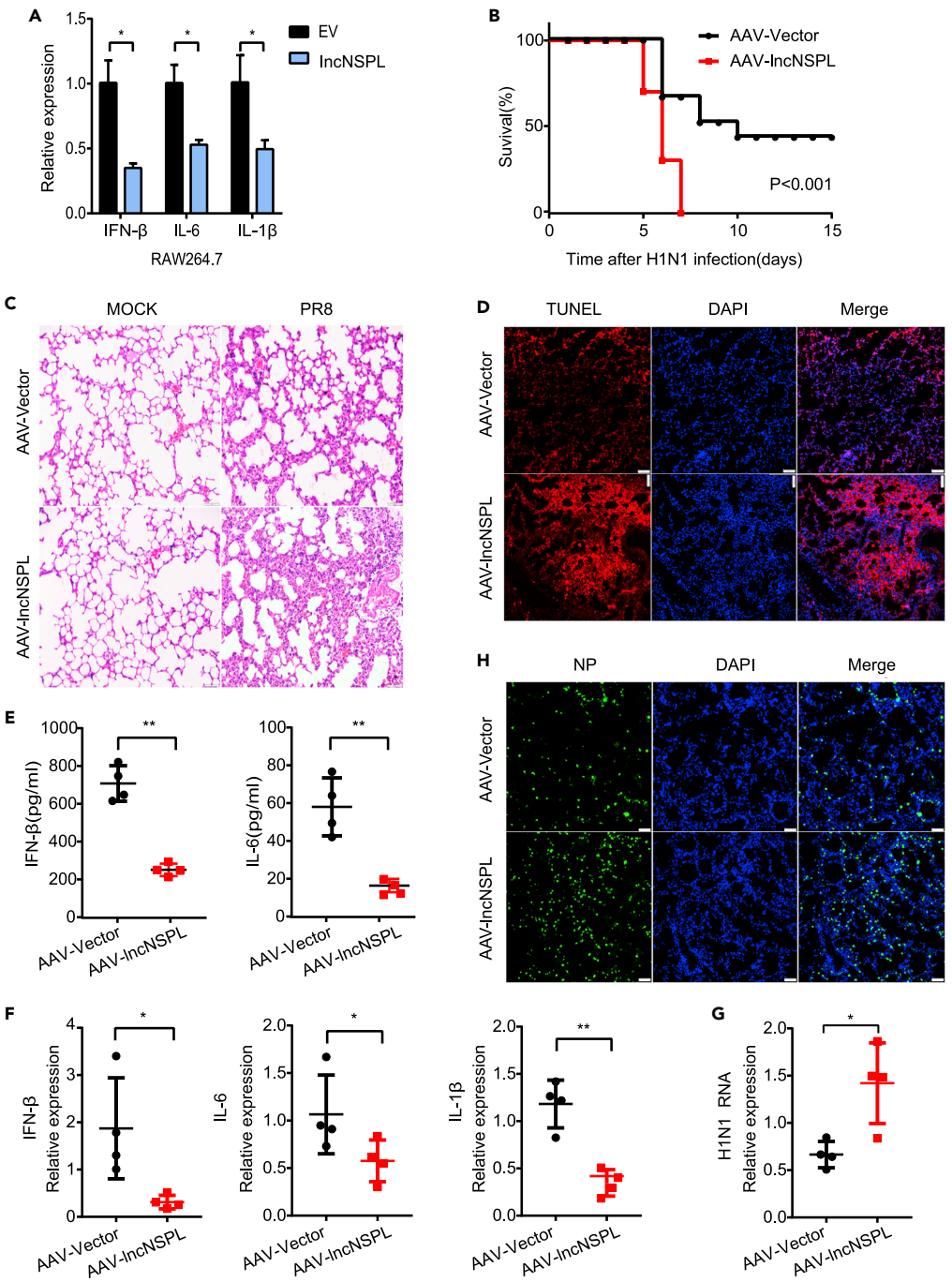

Figure 5. LncNSPL-overexpressing mice are more susceptible to IAV infection with low IFN-I production

(A) qRT-PCR analysis showing the mRNA levels of IFN-β, IL-1β, and IL-6 in RAW264.7 cells transfected with an empty vector (EV) or lncNSPL-overexpressing vector (lncNSPL) for 48 h and infected with H1N1 for 12 h (*$p < 0.05$).

(B) Survival data of six-week-old AAV-lncNSPL mice and AAV-Vector controls (n = 10 per group) 0-15 days after intranasal infection with H1N1 (103 PFU per mouse) (***$p < 0.001$).

(C) HE staining of the lung sections from AAV-lncNSPL and AAV-Vector mice two days after an intranasal infection with H1N1-PR8 (103 PFU per mouse).

(D) Representative images showing the TUNEL stained apoptotic cells (red) in the lung tissue of H1N1-infected AAV-lncNSPL and AAV-Vector mice. Nuclei were stained with DAPI (blue). Scale bar: 50 μm.

(E) ELISA of IFN-β and IL-6 protein levels in the serum of AAV-lncNSPL and AAV-Vector mice as in (B) (**$p < 0.01$).

Figure 5. *Continued*

(F) qRT-PCR analysis of mRNA levels of IFN-β, IL-1β, and IL-6 in the lungs of AAV-lncNSPL and AAV-Vector mice (n = 4 per group) at 48 h after intranasal infection with H1N1 (*$p < 0.05$, **$p < 0.01$).

(G) H1N1 load in the lung tissue of AAV-lncNSPL and AAV-Vector mice (n = 4 per group) 48 h after intranasal infection with H1N1 (*$p < 0.05$).

(H) Immunofluorescence staining was used to measure the expression of the viral NP protein. Scale bar: 50 μm.

with a lethal dose of IAV-H1N1, the AAV-lncNSPL mice were found to be more susceptible to IAV infection, as they displayed a greater mortality rate than the AAV-Vector controls (Figure 5B). When challenged with a moderate dose of IAV-H1N1, the AAV-lncNSPL mice exhibited more severe pathological changes and elevated apoptosis in the lung compared with the AAV-Vector controls (Figures 5C and 5D). The AAV-lncNSPL mice produced decreased levels of IFN-β, IL-1β, and IL-6 in the serum and lung tissue compared to the AAV-Vector controls (Figures 5E and 5F). In line with the decreased IFN-I levels, the AAV-lncNSPL mice displayed elevated IAV-H1N1 replication compared to the AAV-Vector controls (Figures 5G and 5H). Collectively, these observations revealed that lncNSPL-overexpressing mice were more susceptible to IAV infection with low IFN-I production.

LncNSPL directly binds to retinoic acid-inducible gene I helicase and C-terminal domain domains in influenza A virus-infected macrophages

To better understand the molecular mechanism by which lncNSPL regulates RIG-I signaling, we performed an RNA pull-down assay to identify proteins that physically interact with lncNSPL. The lncNSPL-associated proteins were eluted and analyzed by mass spectrometry. RIG-I was the most abundant lncNSPL-binding protein in IAV-infected human macrophages THP-1 (lncNSPL) but did not bind to lncNSPL in the uninfected cells (control) (Figure 6A). This suggested that lncNSPL may inhibit the RIG-I-mediated antiviral innate immune response by directly binding to RIG-I. Consistent with the results of the RNA pull-down assay, the RNA immunoprecipitation (RIP)-qPCR assay also revealed the binding of lncNSPL to RIG-I on IAV infection in an infection time-dependent manner (Figure 6B). In addition, we further verified the lncNSPL-RIG-I binding by displaying the colocalization of lncNSPL with RIG-I by fluorescence *in situ* hybridization (FISH) in IAV-infected THP-1 cells (Figure 6C). In addition, we found that lncNSPL can also bind to mouse RIG-I through an RNA pull-down assay using mouse macrophages RAW264.7 (Figure S14). These results suggest that the direct interaction of lncNSPL and RIG-I exists in both human and mouse immune cells.

RIG-I contains two caspase recruitment domains (CARDs) in the N-terminus, an RNA helicase domain with an ATP-binding motif, and a C-terminal domain (CTD). To further investigate which RIG-I domain interacts with lncNSPL, we performed an *in vitro* RNA pull-down assay with a series of HA-tagged RIG-I truncations (Figure 6D). The result revealed that lncNSPL binds to the wild-type (WT) RIG-I, the CARD1 domain deletion mutant (ΔC1), the CARD2 domain deletion mutant (ΔC2), the 2 CARDs deletion mutant containing helicase and CTD domains (H&C), but fails to bind to the mutant only containing 2 CARDs domains (Figure 6E). These results indicate that RIG-I directly interacts with lncNSPL via its helicase and CTD domains. The RIP-qPCR assay also confirmed the binding of lncNSPL to RIG-I helicase and CTD domains (Figure 6F). A recent series of studies has identified RIG-I and melanoma differentiation-associated gene 5 (MDA5; also called IFIH1) as cytosolic receptors for viral double-stranded RNA and 5 triphosphate RNA. RIG-I and MDA5 both belong to the DExD/H box RNA helicase family, and both have a central helicase domain and a so-called carboxy-terminal domain (CTD) (Yoneyama et al., 2005). To further detect whether lncNSPL could bind to MDA5, and impair the ligand binding of MDA5. RNA pull-down assay indicated that biotinylated lncNSPL was not bound to MDA5 from THP1 cells on H1N1 infection (Figure S15). To identify unique binding sites, we took advantage of the protein structure modeling system to predict the binding element of lncNSPL and map the RIG-I binding region (Figure 6G). Next, we used SWISS-MODEL and RNA structure software to predict and analyze the 3D structure of the RIG-I protein helicase and CTD domains as well as the RNA secondary structure of lncNSPL, respectively. Figure 6H shows a structural visualization of the potential RIG-I-lncNSPL binding complex.

LncNSPL effectively inhibits the K63-linked ubiquitination of retinoic acid-inducible gene I by competing with tripartite interaction motif 25 for retinoic acid-inducible gene I binding

We next investigated how lncNSPL can effectively suppress the RIG-I-mediated innate immune response at the late stage of IAV infection. Interestingly, we found that the level of IFN-β expression (a rapid increase followed by a sharp decrease) did not correlate with a continued increase in RIG-I expression in THP-1

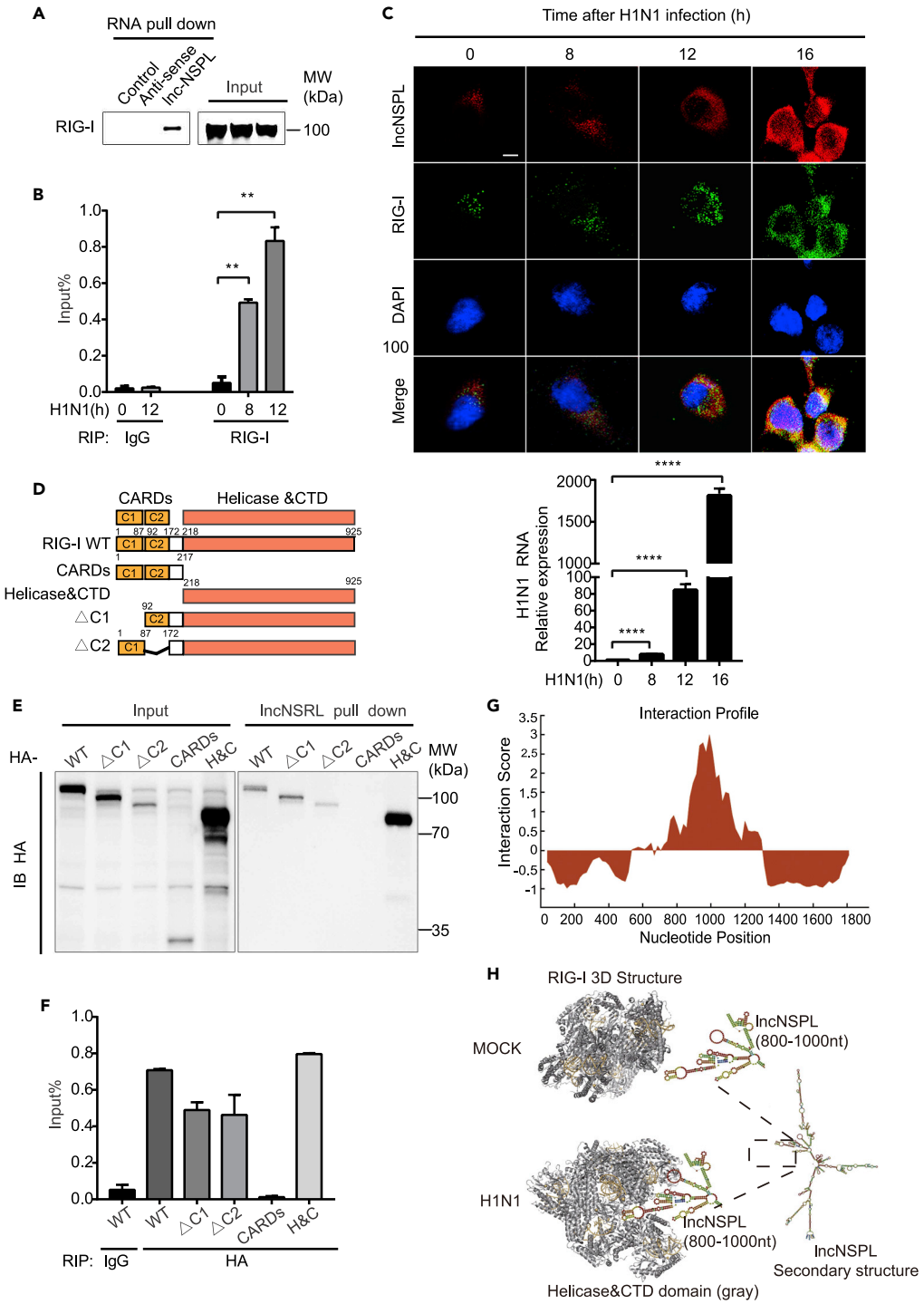

Figure 6. LncNSPL directly binds to RIG-I helicase and CTD domains in IAV-infected macrophages

(A) RNA pull-down assay of in vitro-transcribed lncNSPL binding to RIG-I from THP-1 macrophages infected with IAV.

(B) RIP-qPCR analysis of lncNSPL co-immunoprecipitated with RIG-I from THP-1 cells infected with H1N1 for the indicated time periods (0-12 h) (**$p < 0.01$).

(C) RNA FISH detected endogenous RIG-I (green) and lncNSPL (red) in THP-1 cells infected with H1N1 for the indicated time periods (0-16 h). Nuclei were stained with DAPI (blue) (****$p < 0.0001$). Scale bar: 10 μm.

(D) Schematic of RIG-I and its truncated structures used in the study.

(E) RNA pull-down analysis of the binding of lncNSPL to HA-RIG-I or HA-tagged-truncations of RIG-I.

Figure 6. *Continued*
(F) RIP-qPCR analysis using an anti-HA-antibody in HEK293T cells co-transfected with lncNSPL and HA-RIG-I or HA-tagged-truncations of RIG-I.
(G) Bioanalysis prediction of the binding region of lncNSPL to RIG-I.
(H) Visualization of the interaction between RIG-I and lncNSPL. The 3D structure of RIG-I and the secondary structure model of lncNSPL as simulated using RNA structure software are shown.

macrophages on IAV infection over a period of 16 h and that the rapid decrease of IFN-β was accompanied by a rapid increase in lncNSPL level (Figure 7A). As the expression of lncNSPL gradually increased, the interaction between RIG-I and TRIM25 decreased (Figure 7B). This observation further confirmed that the downstream signal transduction activity mediated by RIG-I was inhibited in the late antiviral reaction. As it was observed that lncNSPL bound to RIG-I on IAV infection (Figures 6A and 6B), we assumed that lncNSPL exerts its function by affecting the interaction between RIG-I and TRIM25. As expected, lncNSPL inhibited the binding of RIG-I to TRIM25 in a dose-dependent manner (Figure 7C). These data suggest that lncNSPL may act as a competitive inhibitor against TRIM25 to bind to RIG-I in IAV-infected cells, thereby dampening the initiation of downstream antiviral signaling including IFN-I production during the later stage of infection. Ubiquitination is a key post-translational modification (PTM) (Pan et al., 2016). It was previously reported that the K63-linked RIG-I polyubiquitination mediated by TRIM25 is essential for its activation (Gack et al., 2007). Thus, we hypothesized that the binding of lncNSPL to RIG-I could inhibit K63-linked ubiquitination. To test this hypothesis, HEK293T cells were co-transfected with HA-tagged full-length RIG-I (HA-RIG-I) together with a Myc-tagged mutant ubiquitin plasmid that only retained the K63 lysine site (Myc-Ub-K63), Flag-tagged TRIM25 (Flag-TRIM25), and/or lncNSPL, before they were infected with IAV-H1N1. The results indicated that lncNSPL overexpression disturbed the TRIM25-mediated K63-linked ubiquitination of RIG-I on IAV infection (Figure 7D). Conversely, knockdown of lncNSPL increased the TRIM25-RIG-I interaction and promoted the TRIM25-mediated K63-linked ubiquitination of RIG-I on IAV infection (Figure 7E). Collectively, these data demonstrate that lncNSPL may assist in the IAV escape from RIG-I-mediated antiviral response by suppressing the interaction between RIG-I and TRIM25 at the late stage of infection (Figure 8).

DISCUSSION

In this study, we identified a novel lncRNA lncNSPL, termed as NS1-promoted lncRNA, that was highly expressed in monocytes of IAV-infected patients and promoted viral replication. At the late stage of IAV infection, viral NS1 protein stimulated the expression of lncNSPL, which directly bound to the RNA sensor RIG-I and suppressed the interaction between RIG-I and TRIM25, leading to the decreased TRIM25-mediated K63-linked ubiquitination of RIG-I. The dampened RIG-I activation then impaired the downstream host anti-IAV innate immune response including RIG-I-induced phosphorylation of NF-κB-P65 and IFN-β activation as well as the production of antiviral cytokines (Figure 8). These findings provide mechanistic insight into how lncNSPL promotes viral survival and immune escape.

LncRNAs display various functions via interactions with DNA, RNA, or proteins. The functional mechanisms are diverse, including lncRNAs that serve as decoys, signals, guides, or scaffolds to regulate transcription, splicing, and nucleic acid degradation (Kopp and Mendell, 2018; Quinn and Chang, 2016). A large body of evidence has demonstrated that innate immune cells utilize lncRNAs to modulate antiviral innate immunity by inhibiting or promoting virus replication (Jiang et al., 2018; Wang et al., 2019). For example, Lnczc3h7a serves as a molecular scaffold for the stabilization of the RIG-I-TRIM25 complex to increase type I IFN production against RNA virus infection (Lin et al., 2019). Moreover, lncRNA NRAV has been reported to regulate the transcription of IFN-stimulated genes during IAV infection (Ouyang et al., 2014); however, whether lncRNAs can be utilized by viruses to avoid elimination via the host immune response remains largely unknown.

Viruses have evolved immune evasion strategies (Zhang et al., 2021). For influenza viruses, the NS1 protein represents the main IFN antagonist and has been shown to antagonize type I IFN production via dsRNA sequestration, interacting with RIG-I, and direct binding to TRIM25 (Gack et al., 2009; Ruckle et al., 2012). However, to the extent of our knowledge, the mechanism by which NS1 inhibits host innate immunity by promoting lncRNA expression has not been studied. In our study, we found that lncNSPL expression was significantly upregulated on NS1 stimulation in a dose-dependent manner, and that the lncNSPL promoter could be activated by the viral NS1 protein (Figures 3A and 3B). As far as we know, our study is the first to

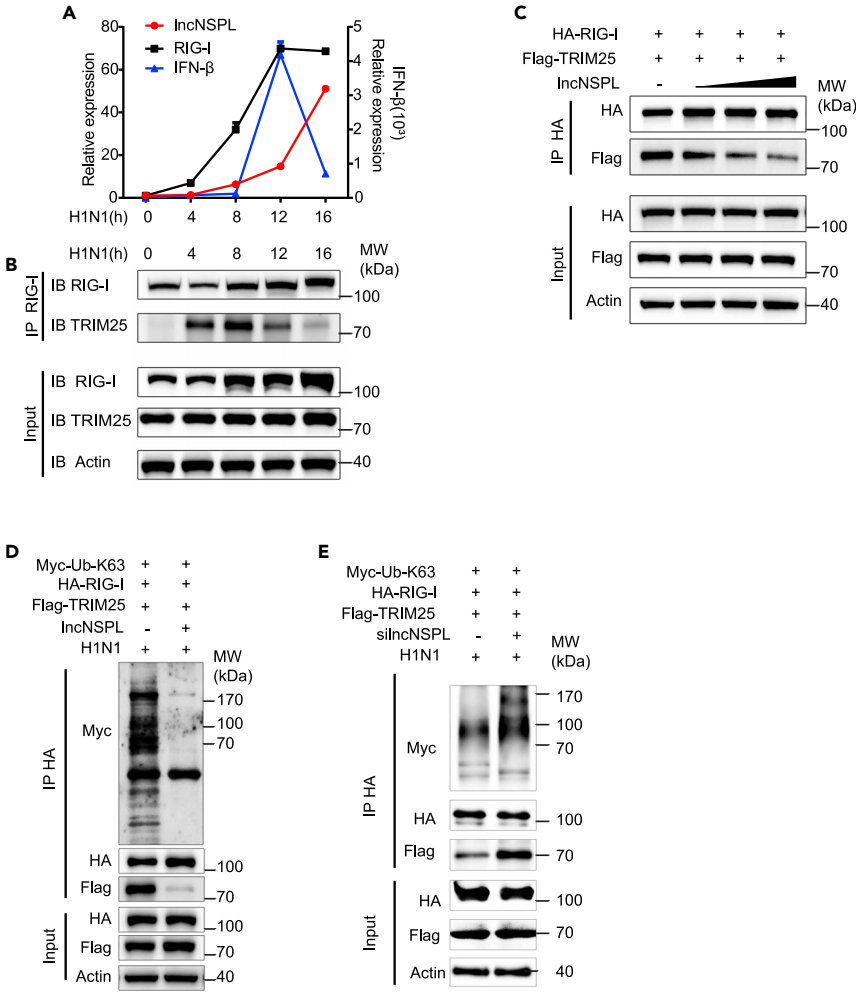

Figure 7. LncNSPL inhibits the K63-linked ubiquitination of RIG-I by competing with TRIM25 for RIG-I binding

(A) Dynamic analysis of mRNA levels of IFN-β, RIG-I, and lncNSPL in H1N1-infected THP-1 cells for the indicated time periods (0-16 h).

(B) Co-immunoprecipitation (Co-IP) analysis of the RIG-I and TRIM25 interaction in the same samples as (A).

(C) Co-IP analysis of the interaction between TRIM25 and RIG-I in HEK293T cells co-transfected with Flag-TRIM25, HA-RIG-I, and the indicated amounts of lncNSPL.

(D) Co-IP analysis of the interaction of TRIM25, RIG-I, and K63-linked ubiquitination of RIG-I in HECK293T cells co-transfected with HA-RIG-I, Flag-TRIM25, Myc-Ub-K63 (a ubiquitin mutant with only K63 available for poly-linkage), with or without lncNSPL followed by H1N1 infection for 12 h.

(E) Co-IP analysis of the interaction of TRIM25, RIG-I, and K63-linked ubiquitination of RIG-I in HECK293T cells co-transfected with HA-RIG-I, Flag-TRIM25, Myc-Ub-K63 (a ubiquitin mutant with only K63 available for poly-linkage), with or without silncNSPL followed by H1N1 infection for 12 h.

demonstrate that NS1 may act as a transcription factor to promote lncRNA expression and disrupt IFN-mediated innate immunity, which ultimately leads to viral replication.

Although a functional analysis of lncRNAs based on competitive binding to inhibit proteins has been reported, the extent to which lncRNAs function through this mechanism remains largely unknown (Liu et al., 2012). In this study, lncNSPL was reported to directly bind to RIG-I on IAV infection but did not bind to RIG-I in uninfected cells. In addition, the binding of lncNSPL to RIG-I was significantly increased, with an increased amount of lncNSPL during the late stage of infection. We hypothesized that owing to the generally low abundance of lncNSPL and the frequent promiscuity of protein-RNA interactions, the extent of the interaction between lncNSPL and RIG-I was not obvious during the early stage of viral

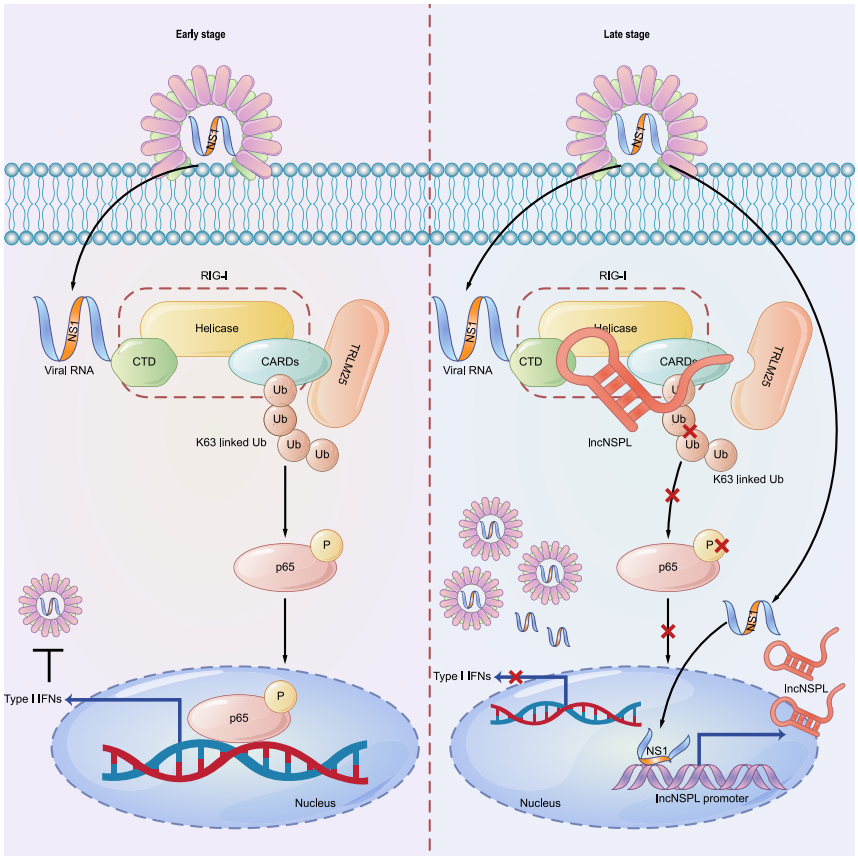

Figure 8. Working model indicating that lncNSPL facilitates influenza A viral immune escape by blocking TRIM25-mediated K63-linked RIG-I ubiquitination Schema summarizing key findings in this study

At the late stage of IAV infection, viral NS1 protein stimulates the expression of lncNSPL, which directly binds to the helicase and CTD domains of RNA sensor RIG-I and suppresses the interaction between RIG-I and TRIM25, leading to the decreased TRIM25-mediated K63-linked ubiquitination of RIG-I. The dampened RIG-I activation then impaired the downstream host anti-IAV innate immune response including RIG-I-induced phosphorylation of NF-κB-P65 and IFN-ββactivation as well as production of antiviral cytokines type I IFNs, leading to elevated viral replication.

infection.TRIM25 is crucial for RIG-I activation and previous studies have shown that the stability of the TRIM25-RIG-I interaction is essential for a sustained antiviral response (Martín-Vicente et al., 2017; Pauli et al., 2014).

RIG-I exists in a closed state in the absence of viral RNA. After viral RNA recognition and binding, RIG-I undergoes a series of structural rearrangements that expose the helicase and CARD domains (Kowalinski et al., 2011). Moreover, the SPRY domain of TRIM25 binds to the exposed CARD domains to mediate ubiquitination (Okamoto et al., 2017). The present data indicate that lncNSPL appeared to bind to the helicase and CTD domains of RIG-I via an RNA stem-loop RNA structure around nucleotides 800-1200 during IAV infection. We assumed that the binding of lncNSPL to RIG-I may restrict the RIG-I protein conformation shift, thereby making RIG-I lose its ability to bind TRIM25. We noted that the isolated structure containing the helicase and CTD domains was a truncation mutant removing both CARDs, maintained in a flexible open conformation, and exposed multipartite RNA-binding sites (Feng et al., 2013). When lncNSPL bound to RIG-I, RIG-I was in an auto-repressed form and the partial RNA-binding sites in the CARD domain were hidden by the interaction between helicase and the CTD domains. Therefore, lncNSPL might obscure the binding sites between RIG-I and TRIM25, thereby preventing the transmission of antiviral signals. Furthermore, the binding of lncNSPL to the helicase and CTD domains of RIG-I may induce a conformational change in the CARDs. Thus, the CARDs could not be exposed to bind with TRIM25 and the ability of RIG-I to bind to TRIM25 was significantly reduced. Consequently, lncNSPL efficiently reduced the TRIM25-mediated K63-linked ubiquitination of RIG-I after IAV-H1N1 infection. In addition, it is unclear

whether there are some novel RIG-I modifications or regulations that have not been revealed. The binding of lncNSPL to RIG-I may also influence these unrevealed regulations to facilitate antiviral innate immunity. Further structural characterization of the RIG-I-lncNSPL complex will reveal the detailed features of this interaction.

Although lncNSPL is not conserved between humans and mice, an RNA pull-down assay indicated that lncNSPL also binds to RIG-I in mice. Our data reveal that lncNSPL overexpression promotes IAV replication and aggravates lung injury in AAV-lncNSPL mice. These results may suggest that the function of lncNSPL in inhibiting IFN-I production might be universal in both humans and mice.

In summary, this study demonstrates the role of NS1-promotion of lncNSPL in IAV immune escape via inhibiting TRIM25-mediated RIG-I activation and preventing the production of IFN-I (Figure 8). These findings broaden our understanding of the molecular mechanisms of lncRNA functions in IAV immune escape. Apart from lncNSPL, we identified 11 other lncRNAs unregulated in IAV-infected monocytes (Figure 2D), which may play roles in antiviral immunity. Characterization of these lncRNAs is, therefore, underway. This study also suggests lncNSPL as a potential therapeutic target in antiviral intervention during IAV infection. Considering its mechanism involving ssRNA sensor RIG-I, the potential clinical implication of lncNSPL may also apply to the infection of other RNA viruses such as SARS-COV-2, which is supported by our finding that coronavirus disease-COVID-19 is one of the most significant pathways associated with lncNSPL and its predicted target genes.

Limitations of the study

In this study, we demonstrated that lncNSPL directly binds the RIG-I, by competing with TRIM25. The detailed molecular mechanism behind LncNSPL inhibits the TRIM25-mediated K63-linked RIG-I ubiquitination still remains to be further investigated.

STAR★METHODS

Detailed methods are provided in the online version of this paper and include the following:

- KEY RESOURCE TABLE
- RESOURCE AVAILABILITY
  - Lead contact
  - Materials availability
  - Data and code availability
- EXPERIMENTAL MODEL AND SUBJECT DETAIL
  - Influenza a virus
  - Cell cultures
  - Human blood samples
  - Details of mice
- METHOD DETAILS
  - Plasmid constructs and small interfering RNAs
  - RNA extraction and gene expression analyses
  - RNA fluorescence *in situ* hybridization (FISH)
  - Northern blotting
  - Enzyme-linked immunosorbent assay (ELISA)
  - Dual-luciferase reporter assay
  - Co-immunoprecipitation
  - Flow cytometry of human peripheral blood mononuclear cells (PBMCs)
  - RNA pull-down assay
  - RNA immunoprecipitation (RIP)
  - Bioinformatics analysis
- QUANTIFICATION AND STATISTICAL ANALYSIS

SUPPLEMENTAL INFORMATION

Supplemental information can be found online at https://doi.org/10.1016/j.isci.2022.104607.

ACKNOWLEDGMENTS

This work was supported by the National Key Research and Development Program of China (2021YFA1301100, 2018YFC2000500), the Key Research & Developement Plan of Zhejiang Province (2019C04005) and the Independent Task of State Key Laboratory for Diagnosis and Treatment of Infectious Diseases (2021).

AUTHOR CONTRIBUTIONS

H.Y.D. and J.J.J. conceived and designed the study; J.J.J., Y.Y.L., X.H.L., F.S., J.Y., Q.Z., Y.T.M., and Y.C.W. performed the experiments and provided discussions; Z.Y.S. and X.H.M. analyzed the data; J.J.J., H.Y.D., and L.G. wrote the article. All authors contributed to the article and approved the submitted version.

DECLARATION OF INTERESTS

The authors declare no competing interests.

Received: December 30, 2021
Revised: April 21, 2022
Accepted: June 9, 2022
Published: July 15, 2022

REFERENCES

Chen, W., Jiang, J., Gong, L., Shu, Z., Xiang, D., Zhang, X., Bi, K., and Diao, H. (2021a). Hepatitis B virus P protein initiates glycolytic bypass in HBV-related hepatocellular carcinoma via a FOXO3/miRNA-30b-5p/MINPP1 axis. J. Experimental. Clin. Can. Res. *40*, 1. https://doi.org/10.1186/s13046-020-01803-8.

Chen, W.B.A., Bi, K.F., Jiang, J.J., Zhang, X.J., and Diao, H.Y. (2021b). Integrated analysis of human influenza A (H1N1) virus infection-related genes to construct a suitable diagnostic model. Bio. Cell *45*, 885–899. https://doi.org/10.32604/biocell.2021.012938.

Chen, X., He, Y., Zhu, Y., Du, J., and Sun, H. (2021c). Linc-AAM facilitates gene expression contributing to macrophage activation and adaptive immune responses. Cell Rep. *34*, 108584. https://doi.org/10.1016/j.celrep.2020.108584.

de Marcken, M., Dhaliwal, K., Danielsen, A.C., Gautron, A.S., and Dominguez-Villar, M. (2019). TLR7 and TLR8 activate distinct pathways in monocytes during RNA virus infection. Sci. Signal. *12*, eaaw1347. https://doi.org/10.1126/scisignal.aaw1347.

Feng, M., Ding, Z., Xu, L., Kong, L., Wang, W., Jiao, S., Shi, Z., Greene, M.I., Cong, Y., and Zhou, Z. (2013). Structural and biochemical studies of RIG-I antiviral signaling. Protein Cell *4*, 142–154. https://doi.org/10.1007/s13238-012-2088-4.

Gack, M.U., Albrecht, R.A., Urano, T., Inn, K.S., Huang, I.C., Carnero, E., Farzan, M., Inoue, S., Jung, J.U., and García-Sastre, A. (2009). Influenza A virus NS1 targets the ubiquitin ligase TRIM25 to evade recognition by the host viral RNA sensor RIG-I. Cell Host. Microbe. *5*, 439–449. https://doi.org/10.1016/j.chom.2009.04.006.

Gack, M.U., Shin, Y.C., Joo, C.H., Urano, T., Liang, C., Sun, L., Takeuchi, O., Akira, S., Chen, Z., Inoue, S., and Jung, J.U. (2007). TRIM25 RING-finger E3 ubiquitin ligase is essential for RIG-I-mediated antiviral activity. Nature *446*, 916–920. https://doi.org/10.1038/nature05732.

Gopal, R., Marinelli, M.A., and Alcorn, J.F. (2020). Immune mechanisms in cardiovascular diseases associated with viral infection. Front. Immunol. *11*, 570681. https://doi.org/10.3389/fimmu.2020.570681.

Haller, O., Kochs, G., and Weber, F. (2006). The interferon response circuit: induction and suppression by pathogenic viruses. Virology *344*, 119–130. https://doi.org/10.1016/j.virol.2005.09.024.

Hou, F., Sun, L., Zheng, H., Skaug, B., Jiang, Q.X., and Chen, Z.J. (2011). MAVS forms functional prion-like aggregates to activate and propagate antiviral innate immune response. Cell *146*, 448–461. https://doi.org/10.1016/j.cell.2011.06.041.

Jiang, F., Ramanathan, A., Miller, M.T., Tang, G.Q., Gale, M., Jr., Patel, S.S., and Marcotrigiano, J. (2011). Structural basis of RNA recognition and activation by innate immune receptor RIG-I. Nature *479*, 423–427. https://doi.org/10.1038/nature10537.

Jiang, M., Zhang, S., Yang, Z., Lin, H., Zhu, J., Liu, L., Wang, W., Liu, S., Liu, W., Ma, Y., et al. (2018). Self-recognition of an inducible host lncRNA by RIG-I feedback restricts innate immune response. Cell *173*, 906–919.e13. https://doi.org/10.1016/j.cell.2018.03.064.

Kopp, F., and Mendell, J.T. (2018). Functional classification and experimental dissection of long noncoding RNAs. Cell *172*, 393–407. https://doi.org/10.1016/j.cell.2018.01.011.

Kowalinski, E., Lunardi, T., McCarthy, A.A., Louber, J., Brunel, J., Grigorov, B., Gerlier, D., and Cusack, S. (2011). Structural basis for the activation of innate immune pattern-recognition receptor RIG-I by viral RNA. Cell *147*, 423–435. https://doi.org/10.1016/j.cell.2011.09.039.

Krug, R.M. (2015). Functions of the influenza A virus NS1 protein in antiviral defense. Curr. Opinion Virol. *12*, 1–6. https://doi.org/10.1016/j.coviro.2015.01.007.

Lai, C., Liu, L., Liu, Q., Wang, K., Cheng, S., Zhao, L., Xia, M., Wang, C., Duan, Y., Zhang, L., et al. (2021). Long noncoding RNA AVAN promotes antiviral innate immunity by interacting with TRIM25 and enhancing the transcription of FOXO3a. Cell Death Differ. *28*, 2900–2915. https://doi.org/10.1038/s41418-021-00791-2.

Lin, H., Jiang, M., Liu, L., Yang, Z., Ma, Z., Liu, S., Ma, Y., Zhang, L., and Cao, X. (2019). The long noncoding RNA Lnczc3h7a promotes a TRIM25-mediated RIG-I antiviral innate immune response. Nat. Immunol. *20*, 812–823. https://doi.org/10.1038/s41590-019-0379-0.

Liu, J., Qian, C., and Cao, X. (2016). Post-translational modification control of innate immunity. Immunity *45*, 15–30. https://doi.org/10.1016/j.immuni.2016.06.020.

Liu, X., Li, D., Zhang, W., Guo, M., and Zhan, Q. (2012). Long non-coding RNA gadd7 interacts with TDP-43 and regulates Cdk6 mRNA decay. EMBO J. *31*, 4415–4427. https://doi.org/10.1038/emboj.2012.292.

Martín-Vicente, M., Medrano, L.M., Resino, S., García-Sastre, A., and Martínez, I. (2017). TRIM25 in the regulation of the antiviral innate immunity. Front. Immunol. *8*, 1187. https://doi.org/10.3389/fimmu.2017.01187.

Mibayashi, M., Martinez-Sobrido, L., Loo, Y.M., Cardenas, W.B., Gale, M., Jr., and Garcia-Sastre, A. (2007). Inhibition of retinoic acid-inducible gene I-mediated induction of beta interferon by the NS1 protein of influenza A virus. J. Virol. *81*, 514–524. https://doi.org/10.1128/JVI.01265-06.

Murray, P.J., and Wynn, T.A. (2011). Protective and pathogenic functions of macrophage subsets. Nat. Rev. Immunol. *11*, 723–737. https://doi.org/10.1038/nri3073.

Nikitina, E., Larionova, I., Choinzonov, E., and Kzhyshkowska, J. (2018). Monocytes and macrophages as viral targets and reservoirs. Int. J. Mol. Sci. *19*, 2821. https://doi.org/10.3390/ijms19092821.

Okamoto, M., Kouwaki, T., Fukushima, Y., and Oshiumi, H. (2017). Regulation of RIG-I activation by K63-linked polyubiquitination. Front. Immunol. *8*, 1942. https://doi.org/10.3389/fimmu.2017.01942.

Ouyang, J., Zhu, X., Chen, Y., Wei, H., Chen, Q., Chi, X., Qi, B., Zhang, L., Zhao, Y., Gao, G.F., et al. (2014). NRAV, a long noncoding RNA, modulates antiviral responses through suppression of interferon-stimulated gene transcription. Cell Host. Microbe. *16*, 616–626. https://doi.org/10.1016/j.chom.2014.10.001.

Palese, P., and Schulman, J.L. (1976). Mapping of the influenza virus genome: identification of the hemagglutinin and the neuraminidase genes. Proc. Natl. Acad. Sci. USA *73*, 2142–2146. https://doi.org/10.1073/pnas.73.6.2142.

Pan, J.A., Sun, Y., Jiang, Y.P., Bott, A.J., Jaber, N., Dou, Z., Yang, B., Chen, J.S., Catanzaro, J.M., Du, C., et al. (2016). TRIM21 ubiquitylates SQSTM1/p62 and suppresses protein sequestration to regulate redox homeostasis. Mol. Cell *61*, 720–733. https://doi.org/10.1016/j.molcel.2016.02.007.

Pauli, E.K., Chan, Y.K., Davis, M.E., Gableske, S., Wang, M.K., Feister, K.F., and Gack, M.U. (2014). The ubiquitin-specific protease USP15 promotes RIG-I-mediated antiviral signaling by deubiquitylating TRIM25. Sci. Signal. *7*, ra3. https://doi.org/10.1126/scisignal.2004577.

Quinn, J.J., and Chang, H.Y. (2016). Unique features of long non-coding RNA biogenesis and function. Nat. Rev. Genet. *17*, 47–62. https://doi.org/10.1038/nrg.2015.10.

Rehwinkel, J., and Gack, M.U. (2020). RIG-I-like receptors: their regulation and roles in RNA sensing. Nat. Rev. Immunol. *20*, 537–551. https://doi.org/10.1038/s41577-020-0288-3.

Richard, M., Fouchier, R.A.M., and Duprex, P. (2016). Influenza A virus transmission via respiratory aerosols or droplets as it relates to pandemic potential. FEMS Microbiol. Rev. *40*, 68–85. https://doi.org/10.1093/femsre/fuv039.

Rückle, A., Haasbach, E., Julkunen, I., Planz, O., Ehrhardt, C., and Ludwig, S. (2012). The NS1 protein of influenza A virus blocks RIG-I-mediated activation of the noncanonical NF-κB pathway and p52/RelB-dependent gene expression in lung epithelial cells. J. Virol. *86*, 10211–10217. https://doi.org/10.1128/JVI.00323-12.

Russell, D.G., Huang, L., and VanderVen, B.C. (2019). Immunometabolism at the interface between macrophages and pathogens. Nat. Rev. Immunol. *19*, 291–304. https://doi.org/10.1038/s41577-019-0124-9.

Tan, X., Sun, L., Chen, J., and Chen, Z.J. (2018). Detection of microbial infections through innate immune sensing of nucleic acids. Annu. Rev. Microbiol. *72*, 447–478. https://doi.org/10.1146/annurev-micro-102215-095605.

Wang, J., Li, X., Wang, Y., Li, Y., Shi, F., and Diao, H. (2022). Osteopontin aggravates acute lung injury in influenza virus infection by promoting macrophages necroptosis. Cell death dis. *8*, 97. https://doi.org/10.1038/s41420-022-00904-x.

Wang, J., Zhang, Y., Li, Q., Zhao, J., Yi, D., Ding, J., Zhao, F., Hu, S., Zhou, J., Deng, T., et al. (2019). Influenza virus exploits an interferon-independent lncRNA to preserve viral RNA synthesis through stabilizing viral RNA polymerase PB1. Cell Rep. *27*, 3295–3304.e4. https://doi.org/10.1016/j.celrep.2019.05.036.

Wynn, T.A., Chawla, A., and Pollard, J.W. (2013). Macrophage biology in development, homeostasis and disease. Nature *496*, 445–455. https://doi.org/10.1038/nature12034.

Yao, J., Lin, C., Jiang, J., Zhang, X., Li, F., Liu, T., and Diao, H. (2021). lncRNA-HEIM facilitated liver fibrosis by up-regulating TGF-β expression in long-term outcome of chronic hepatitis B. Front. Immunol. *12*, 666370. https://doi.org/10.3389/fimmu.2021.666370.

Yoneyama, M., Kikuchi, M., Matsumoto, K., Imaizumi, T., Miyagishi, M., Taira, K., Foy, E., Loo, Y.M., Gale, M., Jr., Akira, S., Yonehara, S., Kato, A., and Fujita, T. (2005). Shared and unique functions of the DExD/H-box helicases RIG-I, MDA5, and LGP2 in antiviral innate immunity. J. Immunol. *175*, 2851–2858. https://doi.org/10.4049/jimmunol.175.5.2851.

Zhang, Q., Meng, Y., Wang, K., Zhang, X., Chen, W., Sheng, J., Qiu, Y., Diao, H., and Li, L. (2021). Inflammation and antiviral immune response associated with severe progression of COVID-19. Front. Immunol. *12*, 631226. https://doi.org/10.3389/fimmu.2021.631226.

Zhang, Q., Zhang, X., Lei, X., Wang, H., Jiang, J., Wang, Y., Bi, K., and Diao, H. (2022). Influenza A virus NS1 protein hijacks YAP/TAZ to suppress TLR3-mediated innate immune response. PLoS Pathog. *18*, e1010505. https://doi.org/10.1371/journal.ppat.1010505.

STAR★METHODS

KEY RESOURCE TABLE

REAGENT or RESOURCE	SOURCE	IDENTIFIER
Antibodies		
anti-RIG-I	Abcam	Cat# ab180675
anti-TRIM25	Abcam	Cat# ab167154; RRID: AB_2721902
anti-MAVS	Cell Signaling Technology	Cat# 3993; RRID: AB_823565
anti-MDA5	Cell Signaling Technology	Cat# 5321S; RRID: AB_10694490
anti-IRF3	Cell Signaling Technology	Cat# 4302, RRID: AB_1904036
anti-pIRF3	Cell Signaling Technology	Cat# 29047; RRID: AB_2773013
anti-p65	Cell Signaling Technology	Cat# 4764; RRID: AB_823578
anti-pp65	Cell Signaling Technology	Cat# 3033; RRID: AB_331284
anti-HA	Cell Signaling Technology	Cat# 3724; RRID: AB_1549585
anti-RIG-I	Santa Cruz Biotechnology	Cat# sc-376845; RRID: AB_2732794
anti-Myc	HUABIO	Cat# EM31105
anti-Flag	HUABIO	Cat# M1403-2
anti-β-actin	HUABIO	Cat# ET1701-80
anti-Influenza A virus NP	Gene Tex	Cat# GTX125989; RRID: AB_11168364
anti-Influenza A virus NS1	Gene Tex	Cat# GTX125990; RRID: AB_11170327
Bacterial and virus strains		
Puerto Rico/8/1981H1N1	State Key Laboratory for Diagnosis and Treatment of Infectious Diseases	N/A
H3N2	State Key Laboratory for Diagnosis and Treatment of Infectious Diseases	N/A
HSV	State Key Laboratory for Diagnosis and Treatment of Infectious Diseases	N/A
HCoV-OC43	State Key Laboratory for Diagnosis and Treatment of Infectious Diseases	N/A
Chemicals, peptides, and recombinant proteins		
LipofectamineTM2000	Thermo Fisher Scientific	Cat#1668-019
Trizol	Invitrogen	Cat#15596026
Penicillin-Streptomycin	Invitrogen	Cat#15140122
Puromycin	Sigma	Cat#P8833
Critical commercial assays		
Pierce™ magnetic RNA-protein pull-down kit	Thermo Fisher Scientific	Cat#20164
RNA Immunoprecipitation kit	Merck Millipore	Cat#17-700
Dual-Luciferase Reporter Assay	Promega	Cat#E1960
RNA Clean & Concentrator	ZYMO RESEARCH	Cat#R1015
T7 RNA polymerase	Thermo Fischer Scientific	Cat#18033019
SP6 RNA polymerase	Thermo Fischer Scientific	Cat#EP0131
HiScript II Q RT SuperMix for qPCR kit	Vazyme	Cat#R222-01
ChamQ Universal SYBR qPCR Master Mix	Vazyme	Cat#Q711-02/03
Fluorescent *In Situ* Hybridization Kit	GenePharma Shanghai, China	Cat#F12202
Annexin V Apoptosis Detection Kit FITC	Thermo Fischer Scientific	Cat#88-8005-72

(*Continued on next page*)

Continued

REAGENT or RESOURCE	SOURCE	IDENTIFIER
Experimental models: Organisms/strains		
C57BL/6 Mice	Chinese Academy of Medical Sciences	N/A
Human blood sample	First Affiliated Hospital, College of Medicine, Zhejiang University,China	N/A
Oligonucleotides		
qPCR primers	See Table S1	N/A
Recombinant DNA		
lncNSPL full length sequence	https://www.ncbi.nlm.nih.gov/nuccore/XR_007083671.1	N/A
Software and algorithms		
GraphPad Prism 5	GraphPad Software Inc	https://www.graphpad.com/
ImageJ Software	Open Source	https://imagej.net/software/fiji/
FlowJo v10	FlowJo LLC	https://www.flowjo.com

RESOURCE AVAILABILITY

Lead contact

Further information and requests for resources and reagents should be directed to and will be fulfilled by the lead contact, Hongyan Diao (diaohy@zju.edu.cn).

Materials availability

All unique/stable reagents generated in this study are available from the lead contact upon request.

Data and code availability

All data reported in this paper will be shared by the lead contact upon request. This paper does not report original code. Any additional information required to reanalyze the data reported in this paper is available from the lead contact upon request.

EXPERIMENTAL MODEL AND SUBJECT DETAIL

Influenza a virus

IAV strain PR8 (Puerto Rico/8/1981H1N1) and recombinant strain PR8 expressing NS1-GFP were kindly provided by Professor Wang (Chinese Academy of Medical Sciences & Peking Union Medical College, Beijing, China). Both strains were grown in allantoic cavities from 10-day-old specific pathogen-free (SPF) embryonated chicken eggs for 72 h at 38°C. The allantoic fluid was collected and tested for HA activity with 0.5% chicken red blood cells. Viral titer was quantified by a standard plaque assay using Madin-Darby canine kidney (MDCK) cells and viral stock was aliquoted and stored at −80°C.

Cell cultures

Human cell lines THP-1, A549, HEK293T and mouse cell line RAW264.7 were obtained from the State Key Laboratory for Diagnosis and Treatment of Infectious Disease, Zhejiang University. Cells were cultured in either RPMI-1640 (for THP-1 cells) or high glucose DMEM (Dulbecco's modified Eagle's medium, for A549, HEK293T and RAW264.7 cells) supplemented with FBS (fetal bovine serum) to a final concentration of 10% and 1% Penicillin/Streptomycin (P/S) cocktail at 37°C with 5% CO_2. THP-1 monocytes are differentiated into macrophages by 24h incubation with 100 ug/mL Phorbol - 12 - myristate 13 - acetate (PMA). All chemicals and reagents were purchased from Sigma-Aldrich unless described specifically.

Cells were infected with IAV strain PR8 at indicated MOI in DMEM for 1h at 37°C. After adsorption, the supernatant was aspirated, and then cells were cultured in DMEM containing 1ug/mL TPCK (L-1-tosylamido-2-phenylethyl chloromethyl ketone)-treated trypsin (Thermo Fisher Scientific) for indicated time at 37°C with 5% CO_2.

Human blood samples

Human blood samples from influenza A virus (IAV)-infected patients and healthy donors were obtained from donors with their informed consent. This study and the usage of these blood samples were approved by the Ethics Committee of the First Affiliated Hospital, College of Medicine, Zhejiang University (Ethics number: 2018–968, 2021–027). A total of 162 IAV-infected patients and 147 healthy donors (HCs) were recruited from the First Affiliated Hospital, College of Medicine, Zhejiang University, between 2018 and 2019. All patients were confirmed to be IAV-positive following the performance of quantitative reverse transcription-PCR (qRT-PCR) assay in throat swabs which utilized specific probes and primers for IAV detection. The summarized patient information was listed in Table S1.

Details of mice

Four-week-old male C57BL/6 mice were purchased from Institute of Laboratory Animal Science, Chinese Academy of Medical Sciences (Beijing, China). The lncNSPL-overexpressing (AAV-lncNSPL) mice on a C57BL/6 background were constructed by infecting C57BL/6 mice with AAV9-lncNSPL (2.5×10^{11} PFU per mouse) via tail intravenous (i.v.) injection. Then 21 days later, mice were infected with IAV-H1N1 strain PR8 (10^3 PFU per mouse) by intranasal (i.n.) injection. All animal experiments were undertaken in accordance with the National Institutes of Health Guide for the Care and Use of Laboratory Animals, and approved by the Ethics Committee of the First Affiliated Hospital, College of Medicine, Zhejiang University (Ethics number: 2021–06). All the animals were generated and housed at specific pathogen-free (SPF) level.

METHOD DETAILS

Plasmid constructs and small interfering RNAs

Sequence of lncNSPL (Gene number: 105370355,accession: XR_007083671), RIG-I and TRIM25 genes were obtained from the NCBI database. The lncNSPL plasmid construction process is divided into two steps. In the first step, the full length of lncNSPL was synthesized and cloned into pUC57 vector (Sangon Biotech, Shanghai, China). And then the full-length lncNSPL was cloned into the pcDNA3.1 eukaryotic expression vector and the retroviral vector GV367 by molecular cloning techniques, respectively. In this retroviral vector construct, lncNSPL transcribed was from RNA Pol II promoter of retroviral vectors GV367. Coding sequences of RIG-I and TRIM25 were cloned into pCDNA3.1 vector containing HA and Flag tags, respectively (Sangon Biotech, Shanghai). HA-tagged truncated structures of RIG-I were generated by standard molecular biology methods. Myc-Ub-K63 structure was a gift from Dr. Q. Zhang (Zhejiang University, China). Full-length lncNSPL was cloned in retroviral vectors GV367 for stable expression in THP-1 cells. LV10 lentiviral vector expressing control shRNA against RFP or shRNA targeting lncNSPL were obtained from Gene Pharma (Shanghai, China).

Small interfering RNAs (siRNAs) were designed and synthesizeds by GenePharma (Shanghai, China). The transfection of plasmids or siRNAs were performed using Lipofectamine 2000 (Invitrogen), according to the manufacturer's instructions.

RNA extraction and gene expression analyses

Total RNA was purified from cells using RNAiso Plus (Takara Bio, Dalian, China). The concentrate of RNA was determined by Nanodrop 2000 (Thermo-Fisher Scientific, USA) and diluted using DEPC-treated water. Equal amount of RNA (250~1000ng) was reverse transcribed using HiScript II Q RT SuperMix for qPCR kit (Vazyme, China). Diluted cDNAs (1: 100 final) were subjected to qPCR analysis using ChamQ Universal SYBR qPCR Master Mix (Vazyme, China) with the following parameters: 95°C for 30 s, followed by 40 cycles of 95 °C for 10 s, 60 °C for 30 s, followed by melting curve analysis. All primers for qPCR (see Table S2) were synthesized by Sangon Biotech (Shanghai). Data were normalized using glyceraldehyde 3-phosphate dehydrogenase (GAPDH) as internal controls and calculated using the $2^{-\Delta\Delta CT}$ method.

RNA fluorescence *in situ* hybridization (FISH)

FISH probes were designed and synthesized by GenePharma (Shanghai, China), and the signals of the probes were detected by a Fluorescent *in Situ* Hybridization Kit (GenePharma, Shanghai, China) according to the manufacturer's instructions. Briefly, cells were fixed in 4% purified formaldehyde (Biological Industries) at room temperature for 15 min and then permeabilized with 0.01% Buffer A for 15 min. Cells were washed in 1 mL of PBS and blocked with 2×buffer C for 30 min at 37 °C. Eight hours of 45 °C hybridization with RNA FISH probes (lncNSPL or RIG-I FISH probes, Gene Pharma) in buffer E was performed followed by

one wash in 2×buffer C for 5 min at 45 °C and DNA staining with DAPI for 10 min at room temperature. Finally, cells were washed in PBS buffer and imaged under confocal fluorescence microscope.

Northern blotting

For northern blotting, total RNA was isolated from THP1 cells using TRIzol reagent. After degeneration for 2 min at 70 °C, equivalent total RNA was separated on a 1.5% denaturing agarose gel and transferred to Hybond N+ membrane. The membrane was prehybridized for 30 min and hybridized with denatured RNA probes at 42 °C for 16 h. Finally, the band was detected using chemiluminescent imaging instrument.

Enzyme-linked immunosorbent assay (ELISA)

Cell culture supernatant or serum samples were collected and the antiviral cytokine levels of IFN-β, IL-6 and IL-1β were measured using enzyme-linked immunosorbent assay (ELISA) kits (Multi Sciences) according to the manufacturer's instructions.

Dual-luciferase reporter assay

Luciferase activity was measured using the Dual-Glo Luciferase Assay System (Promega) following the manufacturer's instructions. Briefly, the mixture of the indicated expression plasmids was co-transfected into HEK293T cells. Then cells were harvested and lysed, subjected to dual-luciferase reporter assay using Dual-Luciferase Reporter Assay System (Promega, cat# E1960). Data were normalized for transfection efficiency by dividing firefly luciferase activity with that of Renilla luciferase.

Co-immunoprecipitation

For co-immunoprecipitation (co-IP), cell extracts were incubated with agitation for 2 h at 4 °C with the indicated antibodies, followed by further incubation with protein A/G beads (Thermo) overnight at 4 °C. The immune complexes were then washed with lysis buffer and subjected to immunoblot analysis.

Flow cytometry of human peripheral blood mononuclear cells (PBMCs)

PBMCs were isolated from collected blood samples and stained with anti-CD14-BV421, anti-CD19-PE, anti-CD3-PE-cy5 and anti-CD56-PE-cy5 antibodies (BD Biosciences). Flow cytometry was performed on BD LSRFortessa X-20 Cell Analyzer (BD Biosciences). Data was collected on BD FACSDiva software v8.0.3 (BD Biosciences) and analyzed using FlowJo software v10.5.3 (TreeStar). PBMCs were gated to identify the lymphocyte population based on forward and side scatter, followed by gating for single cell and live cell populations. Unstained, single color, and fluorescence-minus-one control were used to identify stained populations of cells of interest.

RNA pull-down assay

Linearized pUC57 vector (Sigma-Aldrich) expressing lncNSPL was used as a template to synthesize lncNSPL or its antisense (AS) control RNA. LncNSPL or its antisense (AS) control RNA were *in vitro* transcribed using T7 polymerase (Life Technology). Newly synthesized RNAs were purified with RNA Clean & Concentrator kit (ZYMO RESEARCH) and then labeled with Pierce RNA 3′ Desthiobiotinylation Kit (Thermo Scientific). Streptavidin magnetic beads were washed and incubated with *in vitro*-transcribed biotin-tagged RNAs for 30 min at room temperature followed by washing three times with 20 mM Tris (pH 7.5). Cells were harvested and lysed with Pierce IP Lysis Buffer (Thermo Scientific) with final protein concentration of the cell lysate above 2 mg/mL. Cell lysates were incubated with the RNA-bound beads with agitation overnight at 4 °C. Beads were then washed briefly with 1 mL wash buffer for three times and the eluted proteins were detected by mass spectrometry or boiled in SDS buffer for 10 min at 95 °C, followed by immunoblot analysis.

RNA immunoprecipitation (RIP)

RIG-I antibody (Abcam) or negative control antibody of the same species were incubated with protein A/G magnetic beads with rotation for 30 min at room temperature. THP-1 cells were infected with IAV-H1N1 for the indicated time periods. Cell lysates were freshly prepared and added to each binding reaction with Protease/Phosphatase Inhibitor Cocktail and RNase inhibitor, and then the mixture was incubated overnight at 4°C with rotation. After washing thoroughly for three times, RNA was eluted and purified using Magna RIP™ kit (Millipore). Total cDNA was synthesized using HiScript II Q RT SuperMix for qPCR kit (Vazyme, China) and analyzed by qPCR.

Bioinformatics analysis

The research data of IAV-infected patients and healthy controls (HCs), containing the expression profiles of RIG-I, TLR7 and TLR8, were downloaded from the GEO database, including cohort GSE38900 (patients: HCs = 16 : 31), cohort GSE100150 (patients: HCs = 25 : 14) and cohort GSE6884. Data processing was as follows: (1) Use the Combat function of the SVA R package to remove batch effects; (2) The normalize between arrays function of the Limma R package was used to normalize, and then the expression spectrum data is $\log_2$ transformed. We obtained 25,435 genes corresponding to 41 influenza sample and 45 normal sample. Limma R package was used for differentially expressed gene (DEG) analysis to obtain the differentially expressed genes in influenza VS normal. The median of RIG-I expressed values was used to distinguish high and Low expressed samples, and the difference between high and low groups was analyzed by Limma R package. The expression profiles of three genes TLR7, TLR8 and RIG-I were extracted from the GEO combined data of the two groups (GSE38900 and GSE100150). The NetworkD3 R packages were used to depict the alluvial diagram of mRNA and corresponding KEGG pathways. We searched for the interaction between genes from pathways based on the string database (score >0), and constructed RIG-I-KEGG regulatory network using Cytoscape software. Student's *t* test and Wilcoxon test were performed to assess the differences in variance between indicators for normally distributed and non-normally distributed data respectively. The Kaplan–Meier (KM) method was used to depict the survival curve and estimate the survival probability of patients which was further examined by the log rank test. The accuracy and sensitivity of survival prediction were verified by receiver operating characteristic (ROC) curve analysis and determined by value of area under curve (AUC). The expression profiles of RIG-I and differential lncRNA were extracted from the raw data, and the correlation analysis was performed by Hmisc R package, and the correlation and significance between RIG-I and differential lncRNA expression were demonstrated by scatterplot. The association between lncRNA from KEGG and predicted genes were revealed through the Hmisc R package. The function of KEGG and GO were analyzed by ClusterProfiler R package and GO plot R package respectively. For statistical analyses, SPSS software and R package were used, and $p < 0.05$ was considered statistically significant.

QUANTIFICATION AND STATISTICAL ANALYSIS

Statistical significance of differences between two experimental groups were carried out using unpaired Student's *t* test in GraphPad Prism 7.0 software and a two-tailed (ns, $p > 0.05$; *, $p < 0.05$; **, $p < 0.01$; ***, $p < 0.001$; ****, $p < 0.0001$) was taken to indicate statistical significance. Data are presented as mean $\pm$ SD of one representative experiment of at least three independent experiments showing similar results.